2024-10-28

Automation, Improvement, and Sensitivity Analysis of 3D Parameterized Maize Stalk Models

Joseph Steven Carter
Brigham Young University

Automation, Improvement, and Sensitivity Analysis of 3D Parameterized Maize Stalk Models

Joseph S. Carter

A thesis submitted to the faculty of
Brigham Young University
in partial fulfillment of the requirements for the degree of

Master of Science

Douglas D. Cook, Chair
John Salmon
Brian Jensen

Department of Mechanical Engineering

Brigham Young University

Automation, Improvement, and Sensitivity Analysis of 3D Parameterized Maize Stalk Models

Joseph S. Carter
Department of Mechanical Engineering
Master of Science

BYU Engineering

Abstract

Maize is the most grown crop in the world. Each year, 5% of maize is lost due to a phenomenon known as stalk lodging (breakage of the stalk below the ear). One of the most promising solutions to stalk lodging is to design stalks with superior geometry to increase stalk strength. Researchers have developed a 3D parameterized maize stalk model, but these models take a long time to structurally analyze and are missing important material properties. This thesis addressed these problems by developing an automated package for analyzing the 3D parameterized maize stalk model, and by measuring the longitudinal shear modulus of both pith and rind stalk tissues. This thesis also identified the most influential geometric patterns in the 3D parameterized maize stalk model, which can be used to breed stronger maize. The results of this thesis are an increased understanding of the factors that influence stalk lodging, and geometric details for how stronger maize can be designed.

Keywords: sensitivity analysis, finite element analysis, biomechanics

Acknowledgments

I would first like to acknowledge the Crop Biomechanics Lab sponsors and the USA National Science Foundation (Award 2046669). Their financial support to the lab has given me the opportunity to perform exciting research while obtaining a degree.

I would like to express my gratitude for my mentor, Dr Douglas Cook. He shows genuine care for me as a person. He has helped me become a better researcher and person.

I would like to acknowledge the students who have helped me complete my work. Michael Ottesen, the student who preceded me, helped me learn Abaqus, the finite element software used in my work. Braxton Fjeldsted, an undergraduate researcher, helped me take measurements for the shear modulus torsion testing found in this thesis. I express gratitude to both of these researchers for helping me with this project.

Finally, I express gratitude to my wife Sophie. Her support for me during my graduate and undergraduate work helped me get to where I am today.

Table of Contents

List of Figures

List of Tables

1 Introduction

1.1 Problem

Maize is the most produced crop in the world [1]. It accounts for 95% of feed in the United States, occupying over 90 million acres of farmland each year [2]. It also comprises 94% of ethanol production [3], which is a major source of fuel in the world. Maize and its byproducts are a major part of the world market. Because of this, any issue in the growth or harvest of maize has a long and lasting impact. One such problem is stalk lodging.

Stalk lodging is the breakage of maize stalks below the ear, and is often caused by wind (see Fig. 1.1). This can lead to harvesting problems and can significantly impact crop yield. It has been estimated that 5% of maize is affected by stalk lodging each year [4], most often at the time of peak maturity. The failure process associated with stalk lodging is complex and depends on many factors. Research on this phenomenon has focused on environmental effects [5], rapid phenotyping [6], and stalk morphology [7], among others.

Figure 1.1: Stalk lodging in a field near Ames, Iowa, October 2019.

One of the most promising areas of study into stalk lodging is the correlation between stalk geometry and strength [8]. It has been theorized that modification to the morphological factors of maize stalks

[1] USDA, "Grain: World Markets and Trade," 2024.

[2] USDA, "Feed Grains Sector at a Glance," 2023.

[3] Energy, "Ethanol Fuel Basics," 2024.

[4] Duvick, "The Contribution of Breeding to Yield Advances in maize," 2005.

[5] Thompson *et al.*, "Corn stover for bioenergy production: Cost estimates and farmer supply response," 2014.

[6] Robertson *et al.*, "An Improved Method for Accurate Phenotyping of Corn Stalk Strength," 2014.

[7] Von Forell *et al.*, "Preventing lodging in bioenergy crops: a biomechanical analysis of maize stalks suggests a new approach," 2015.

[8] Robertson *et al.*, "Maize Stalk Lodging: Morphological Determinants of Stalk Strength," 2017.

could decrease stalk lodging [7]. In order to provide support for this theory, finite element modeling techniques have been applied to maize stalk models to find a relationship between stalk geometry and stalk strength [7, 9–11].

This thesis will continue the use of finite element modeling to characterize how maize stalk material constants and morphology influence strength. The sections below will describe the modeling approaches that have been used in the past to predict maize stalk behavior.

[7] Von Forell *et al.*, "Preventing lodging in bioenergy crops: a biomechanical analysis of maize stalks suggests a new approach," 2015.

[7] Von Forell *et al.*, "Preventing lodging in bioenergy crops: a biomechanical analysis of maize stalks suggests a new approach," 2015.

[9] Ottesen *et al.*, "A parameterised model of maize stem cross sectional morphology," 2022.

[10] Stubbs *et al.*, "Maize stalk stiffness and strength are primarily determined by morphological factors," 2022.

[11] Ottesen *et al.*, "Development and Stochastic Validation of a Parameterized Model of Maize Stalk Flexure and Buckling," 2023.

1.2 Modeling Background

Maize stalks are composed of two materials: a hard outer rind and a soft inner pith. An important characteristic of both of these materials is the presence of inner fibers, which results in non-isotropic behavior. This means that both the pith and rind can be modeled as transverse isotropic materials, which require twelve material constants (ten of which are independent) to fully define [12].

[12] Hashmi *et al.*, *Comprehensive Materials Processing*, 2014.

Relatively little research into maize stalk material constants has been conducted. Although data regarding maize stalk material constants are scarce, some of the twelve material constants have been measured previously. Notable studies include Stubbs [10], who measured transverse elastic modulus of pith and rind tissue; Al-Zube [13], who measured longitudinal elastic modulus of rind tissue; Zhang [14, 15], who measured longitudinal elastic modulus of pith and rind tissue; and Sutherland [16], who measured longitudinal elastic modulus of rind tissue. These constants have been used in a variety of applications, including analytic modeling and finite element analysis.

[10] Stubbs *et al.*, "Maize stalk stiffness and strength are primarily determined by morphological factors," 2022.

[13] Al-Zube *et al.*, "The elastic modulus for maize stems," 2018.

[14] Zhang *et al.*, "Tensile Properties of Maize Stalk Rind," 2016.

[15] Zhang *et al.*, "Mechanical Behavior of Corn Stalk Pith: an Experimental and Modeling Study," 2017.

[16] Sutherland *et al.*, "The Influence of Water Content on the Longitudinal Modulus of Elasticity of Maize Stalk Tissues," 2022.

Maize stalks follow a growth pattern of nodes followed by internodal regions (see Fig. 1.2). Nodal regions have a higher proportion of rind and are generally more resistant to damage than internode regions. It has been found that the vast majority of failure occurs in the region just 4 cm above the node [17].

[17] Robertson *et al.*, "Maize Stalk Lodging: Flexural Stiffness Predicts Strength," 2016.

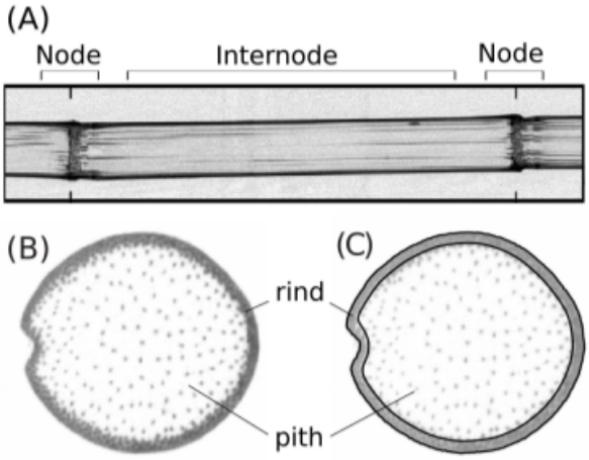

Figure 1.2: Maize stalk physiology, from Ottesen [9].

Various finite element modeling techniques have been used to predict the behavior of maize stalks. Beginning models were created by CT-scanning maize stalks along their length and then reconstructing the geometry using SolidWorks (Dassault Systèmes SE, Vélizy-Villacoublay, France). These high fidelity models were then imported into finite element analysis programs and analyzed for flexural stiffness and failure strength testing (see Fig. 1.3). These first studies suggested that geometry has a more important role on stalk strength than material constants [7].

[7] Von Forell *et al.*, "Preventing lodging in bioenergy crops: a biomechanical analysis of maize stalks suggests a new approach," 2015.

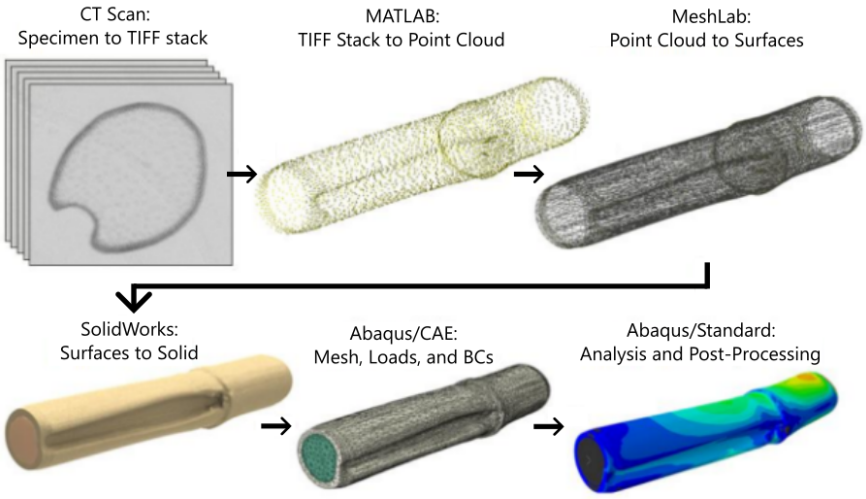

Figure 1.3: CT scan-based models, from Stubbs [10].

Because the CT-scan models indicated such a high dependence of stalk strength on geometry, it was theorized that making small changes to stalk geometry could increase resistance to stalk lodging. In order to support this theory, researchers needed a 3D model of maize stalks with geometry that could be manipulated manually. This could not be done with CT-scan models, as they were specimen-specific, and could not be easily manipulated. Researchers needed a simplified model that could be used to more directly control geometric parameters to see how they affected response.

Simplifying the maize stalk model began with creation of 2D parameterized stalk section models. Principal component parameterization of these models resulted in elliptical cross sections, which were simpler than their CT scan counterparts (see Fig. 1.4). It was found that modeling the cross sections of the stalks as ellipses produced FEA responses that were indistinguishable from those of the CT scan cross sections [9].

[9] Ottesen *et al.*, "A parameterised model of maize stem cross sectional morphology," 2022.

These 2D parameterized ellipse models were also used to create 3D prismatic models for analysis in FEA. This analysis was an important stepping stone to create simpler maize stalk models, but due to their prismatic nature, did not contain important features found in maize stalks such as node and internode regions. The problem still remained: researchers needed a 3D model that was simple enough to understand but complex enough to have high accuracy.

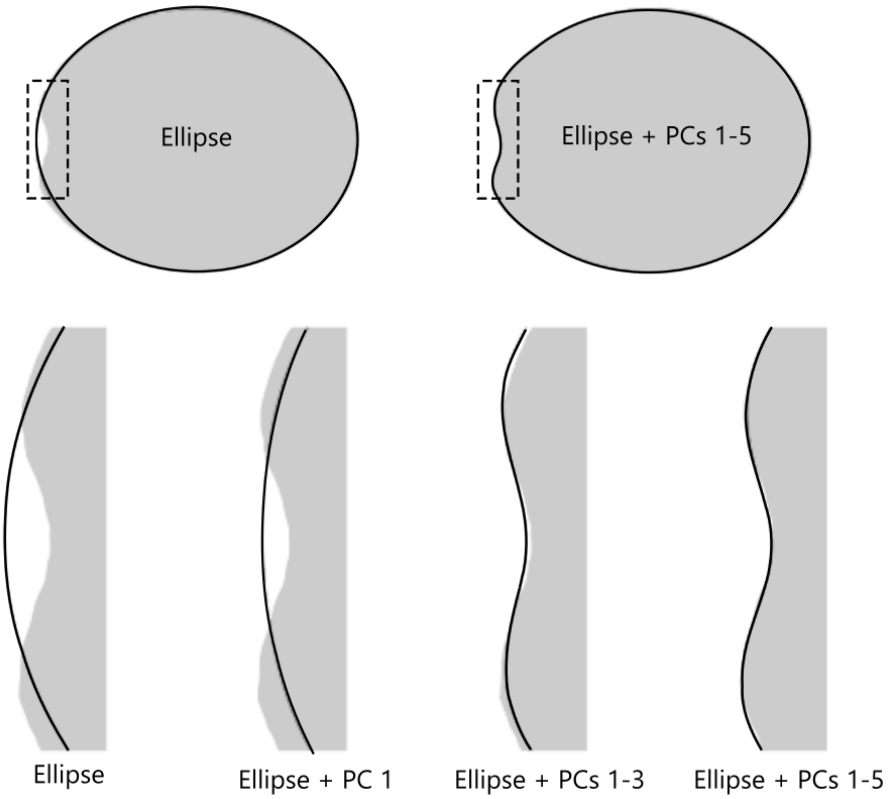

Figure 1.4: Ellipse assumption, from Ottesen [9].

1.3 The 3D Parameterized Maize Stalk Model

Ottesen [18] was the first researcher to develop a 3-dimensional parameterized maize stalk model. These models were created using CT data, but were simplified using an ellipse assumption [9] and parameterization (see Fig. 1.5). Consistent features from over 900 CT-scans were identified, and principal component analysis (PCA) was used to create models with 51 distinct parameters.

The 3D parameterized stalk model was validated by simulating three point bending tests in FEA and comparing these results to physical three point bending tests conducted in a previous study [13, 19].

The 3D parameterized maize stalk model is a powerful tool for understanding the stalk lodging problem. It allows for direct control over geometric parameters while still preserving the behavior of actual maize stalks. This opens the door to sensitivity studies, which will inform researchers of which specific geometric maize stalk features contribute to stalk flexural stiffness, failure strength, and biomass.

[18] Ottesen *et al.*, "Development and stochastic validation of a parameterized model of maize stalk flexure and buckling," 2023.

[9] Ottesen *et al.*, "A parameterised model of maize stem cross sectional morphology," 2022.

[13] Al-Zube *et al.*, "The elastic modulus for maize stems," 2018.

[19] Al-Zube *et al.*, "Measuring the compressive modulus of elasticity of pith-filled plant stems," 2017.

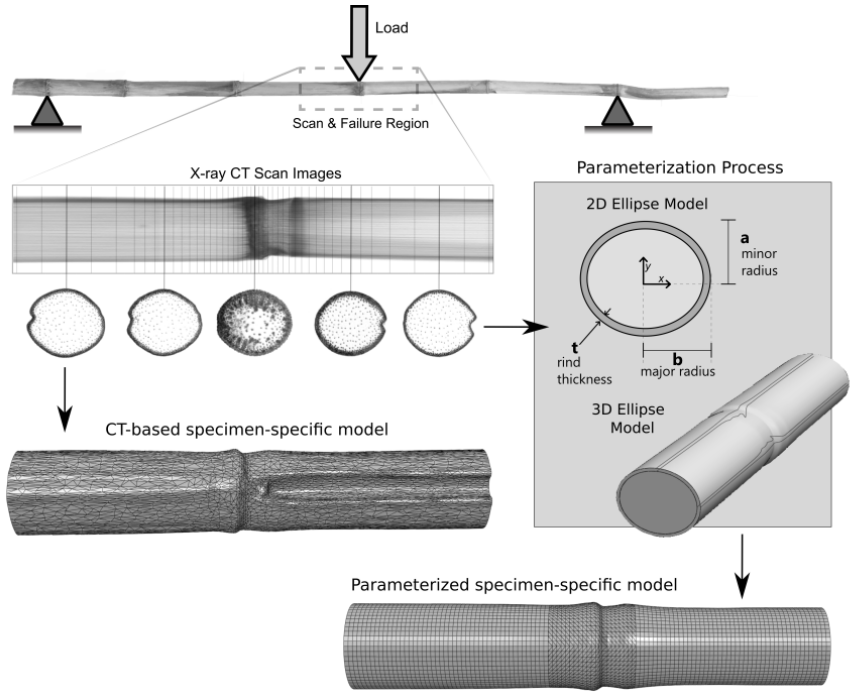

Figure 1.5: Parameterization by Ottesen [18] based on the ellipse assumption and PCA parameterization.

1.4 Purpose

The purpose of this research is to better understand the factors that influence maize stalk strength. This involves three main objectives:

1. Improve and automate the process of creating and analyzing finite element models of the maize stalk;
2. Measure mechanical tissue properties that have not previously been reported;
3. Understand the relationships between material/geometric properties and model flexural stiffness, failure strength, and biomass.

These objectives will gain new knowledge concerning maize stalks that can be used to decrease stalk lodging.

Objective 1: Improve and automate the process of creating and analyzing finite element models of the maize stalk.
Finite element analysis is used to solve for flexural stiffness and failure strength of the 3D parameterized maize stalk model. This requires many operations such as importing the geometry, applying boundary conditions, assigning material constants, and applying finite element meshes. Previously, this process was done manually by an experienced researcher.

Future studies using this automation process will involve creating thousands of finite element models. This means that it is of utmost importance that the analysis of the 3D parameterized maize stalk model be automated. This automation is the subject of Chapter 2.

Objective 2: Measure mechanical tissue properties that have not previously been reported.
This thesis will further improve the 3D parameterized maize stalk model by measuring two material constants that are involved in their use in finite element analysis. These material constants are the longitudinal shear modulus of both the pith and rind tissue. The measurement of these material constants is the subject of Chapter 3.

Objective 3: Understand the relationships between material/geometric properties and model flexural stiffness, failure strength, and biomass.
The geometry of maize stalks is a promising factor involved in stalk lodging. Using the 3D parameterized maize stalk models, we can quantify the relationship between specific geometric features of these models and model response (flexural stiffness, failure strength, and biomass) through sensitivity analysis. This sensitivity analysis will also characterize the relationship between model biomass and failure strength sensitivities. This is of particular interest for future optimization studies, where it may be desired to increase model failure strength without substantial increases in biomass. The sensitivity analysis of model response to geometric and material parameters is the subject of Chapter 4.

Anticipated Outcomes:
The results of this research will be an improved and automated version of the 3D parameterized maize stalk model, and evidence supporting the relationship between maize stalk geometry and stalk behavior. The results of sensitivity analysis will be used as direct evidence supporting whether or not maize stalk geometry could be efficiently leveraged to decrease stalk lodging. These insights will help researchers more effectively address the problem of stalk lodging, which will increase yearly maize yield.

2 *Finite Element Model Automation and Validation*

The 3D parameterized maize stalk model allows for complete control of all model parameters. The method by which these models are structurally analyzed is finite element analysis (FEA). FEA operates by dividing a geometry into small elements, which discretizes the problem into a system of equations that can be solved iteratively. In order to solve this system of equations, a user needs to define many finite element program parameters.

Creating a finite element model in any situation is an involved process: the researcher must manually define all necessary material constants, boundary conditions, and meshes (dividing up the geometry into small elements) to receive structural responses. Even when a researcher gets FEA results, a great deal of post processing is often necessary.

Setting up and processing finite element models is time-consuming, especially when thousands of models are required. To address this, the FEA process for the 3D parameterized maize stalk model was automated. This chapter details the automation process, resulting in a package that will be used in future studies.

2.1 Stalk Geometry Generation

This chapter explains how the structural responses of maize stalk geometries were calculated. This chapter does *not* address how the maize stalk geometries were generated. Instead, we refer to a previous study by Ottesen, who developed the geometry generation approach [9, 11]. Ottesen's approach was used to generate two solid geometries for each stalk: one for the pith (the inner stalk), and one for the rind (the outer stalk). These geometries were generated in SolidWorks .STEP format (Dassault Systèmes SE, Vélizy-Villacoublay, France). Ottesen's geometry generation technique functions separately from the automation technique outlined in this chapter. As such, all geometries needed to be generated before any finite element operations were applied to them.

[9] Ottesen *et al.*, "A parameterised model of maize stem cross sectional morphology," 2022.

[11] Ottesen *et al.*, "Development and Stochastic Validation of a Parameterized Model of Maize Stalk Flexure and Buckling," 2023.

2.2 The Automation System

Automation was implemented using the procedural programming paradigm. Procedural programming achieves an objective through a series of steps called functions [20]. Each function has a specific role in computing a global result. This allows a programmer to write only a few functions that are reused for every new set of inputs, without having to rewrite code for a new situation.

[20] Blokdyk, *Procedural Programming A Complete Guide*, 2020.

Procedural programming was applied to this problem by creating a list of functions that could create a maize stalk geometry, import the geometry into Abaqus 2022 (Systemes Simulia Corporation, Providence, RI, USA), apply all conditions necessary for analysis, run an analysis, and then extract analysis results. These functions were written in Python and executed via the Abaqus 2022/Python interface.

The automation system consisted of two main parts. First, one file contained all of the data required to define a model (inputs.py). This included the stalk CAD file path, material constants, boundary condition configuration, and others. Second, several functions processed the information in inputs.py to create the geometry, boundary conditions, meshes, and analysis. There were eight main subroutines for creating and analyzing maize stalk geometry. The end result was an automated package that can structurally analyze any specified stalk geometry at the push of a button, with complete control over material properties, boundary conditions, and analysis type. A diagram of the code functions that constitute the automation system is provided in Fig. 2.1. The following sections detail the purpose and functionality of each subroutine.

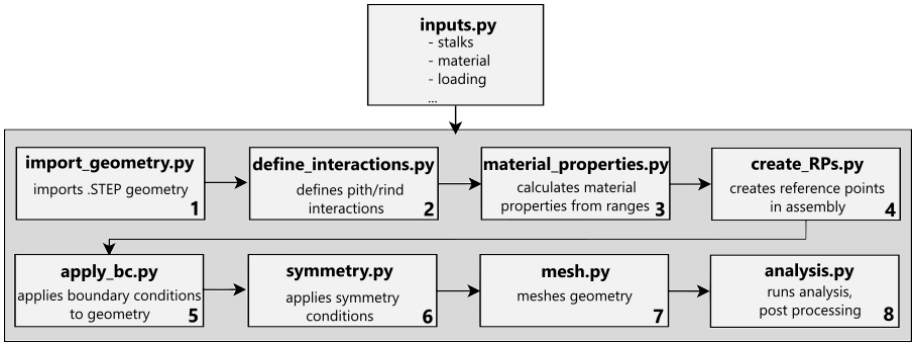

Figure 2.1: Code automation flowchart. This is a simplified version of the actual code. The diagram above shows the general layout that aligns with the sections below.

2.2.1 Subroutine 1: Importing .STEP files

The first subroutine imported a pre-generated stalk geometry into Abaqus 2022. This geometry was manipulated in later subroutines to have user-specified boundary conditions, constraints and material constants for simulation purposes. In addition, this subroutine added guiding lines to the geometry for easier meshing. These lines were drawn based on coordinate axes. Fig. 2.2 shows examples of the imported .STEP files.

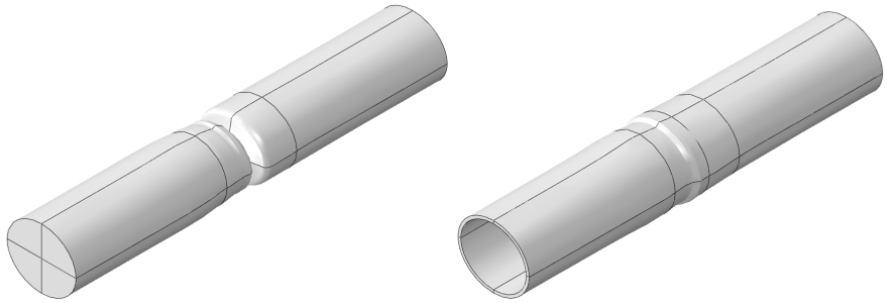

Figure 2.2: STEP files. Pith on the left, rind on the right.

2.2.2 Subroutine 2: Interactions

A tie constraint relationship was used to characterize the interaction between pith and rind. A tie constraint restricts the movement of the secondary surface, ensuring that it matches the displacement of the primary surface. Because the rind controls the majority of stalk behavior, the inner rind was defined as the primary surface, and the outer pith was defined as the secondary surface.

2.2.3 Subroutine 3: Defining Material Constants

The third subroutine defined and applied material constant definitions to the imported geometry. Both the pith and rind were modeled as transverse isotropic materials. A transverse isotropic material has six material constants, five of which are independent. Fig. 2.3 illustrates these six material constants, which are also listed in Table 2.1.

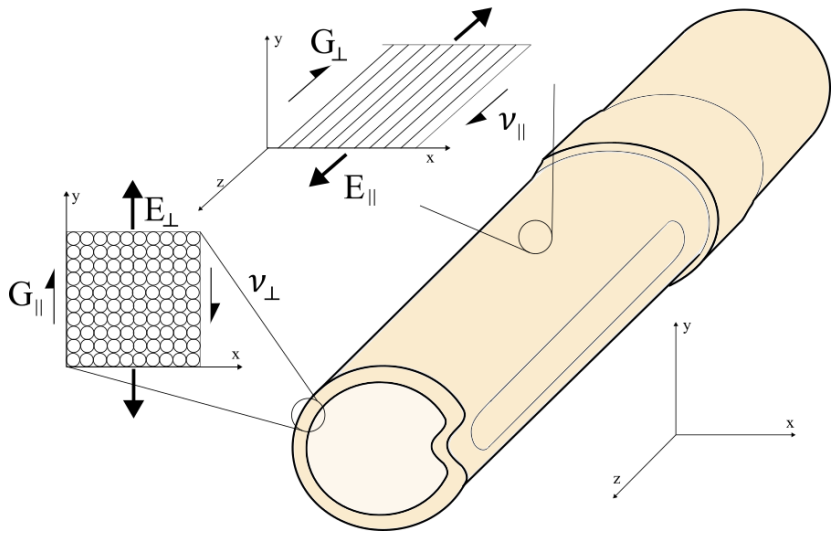

Figure 2.3: Interpretation of transverse isotropy material constants. The || symbol indicates a property in the fiber direction, while the ⊥ symbol indicates a property perpendicular to the fibers. Material direction is highlighted for the rind tissue, but this orientation is also present in pith tissue.

To accurately model the material response of maize stalks, twelve different material constants were required, ten of which were independent. Table 2.1 lists the ranges used in this study for each of these material constants along with their sources.

Table 2.1: Material constant ranges for maize stalk pith and rind tissue, from Ottesen [18]. Units in GPa.

property	method	distribution	pith	rind	source
$E_{\perp}$	random sampling	normal	(0.026, 0.01)	(0.85, 0.39)	Stubbs [10]
rind $E_{\|\|}$	specimen specific	empirical	n/a	specimen specific	Al-Zube [13]
pith $E_{\|\|}$	random sampling	normal	(0.45, 0.05)	n/a	Sutherland [16]
$G_{\perp}$	calculated	n/a	$\frac{E_{\perp}}{2(1+\nu)}$		theory
$G_{\|\|}$	random sampling	normal	(0.27, 0.01)	(0.93, 0.33)	Carter [25]
$\nu_{\perp}$	random sampling	uniform	(0.2, 0.45)		Green [21]
$\nu_{\|\|}$	random sampling	uniform	(0.009, 0.086)		

Due to uncertainty in several properties, a variance test was performed to determine relative influence of each material constant. This involved testing 63 stalks with 10 replicates per stalk. Each replicate was randomly sampled within the bounds listed in Table 2.1, except for $E_{||}$ in the rind, which was taken from stalk-specific physical testing [19]. The results of this test are discussed further in Section 2.3.3.

[19] Al-Zube *et al.*, "Measuring the compressive modulus of elasticity of pith-filled plant stems," 2017.

2.2.4 Subroutine 4: Reference Points

Specific reference points were added to each stalk on the vertices shown in Fig. 2.4. A tie constraint was used for reference points on the end faces, while a rigid body constraint with radii of effect was applied to the reference points in the nodal region. These interactions best mimic physical testing conditions. These reference points are used to easily apply loads and boundary conditions, which are discussed in Section 2.2.5.

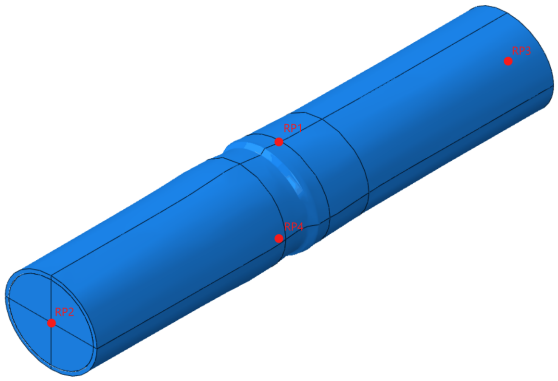

Figure 2.4: Reference point locations on maize stalk geometries.

2.2.5 Subroutine 5: Loading Cases

One of the main goals of this study was to mimic the same conditions used to test the strength of physical maize stalks. This way, the results of simulated maize stalks (in FEA) could be compared against physical maize stalks for validation. This increases our confidence in the parameterized model.

The physical stalk responses used for this study were ones tested by Al-Zube [13, 19]. Al-Zube tested specimens under three point bending loads. Three point bending loads were applied to each model. Table 2.2 summarizes these boundary conditions.

[13] Al-Zube *et al.*, "The elastic modulus for maize stems," 2018.

[19] Al-Zube *et al.*, "Measuring the compressive modulus of elasticity of pith-filled plant stems," 2017.

Table 2.2: Boundary condition calculations, from Ottesen [18].

Load Type	**Bottom Face**	**Top Face**
Force	$F_a = \frac{M_{fail}}{A}$	$F_b = \frac{M_{fail}}{B}$
Moment	$M_a = \frac{A-a}{A} M_{fail}$	$M_b = \frac{B-b}{B} M_{fail}$
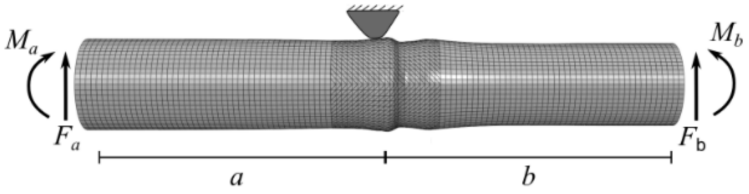		

A	Distance between left-hand support and applied load in the 3-point bending test
B	Distance between the right-hand support and applied load in the 3-point bending test
M_{fail}	Maximum bending moment applied during physical 3-point bending tests

For modeling purposes, only the middle of each stalk was considered in calculations. "A" was the length of the top half of each stalk, "B" was the length of the bottom half of each stalk, and "a" or "b" were the *modeled* section of each of these sections. These test conditions are also shown in Fig. 2.5.

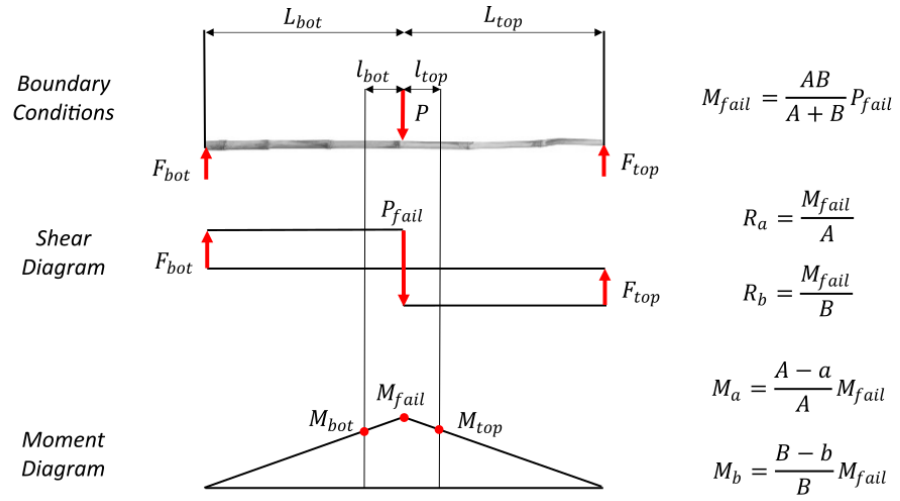

Figure 2.5: Load diagrams for three point bending of maize stalks. Writing in terms of a normalized Pfail yields the equations shown. Loads were normalized by Pfail because the linear buckling analysis requires a scalable input load.

This subroutine applied these loads and moments to the reference points described in Section 2.2.4 and constrained the middle section of each stalk. As will be discussed in Chapter 4, there were also other load configurations applied to each model, but for validation, the load conditions described above were used.

2.2.6 Subroutine 6: Symmetry

To handle potentially long and repetitive tests, simplifying the geometry can significantly reduce processing time. One effective method is to apply symmetry conditions. Because the parameterized maize stalk model has an elliptical cross-section, it has two symmetry planes. A symmetry boundary condition in the yz plane was used to simplify the model and reduce computational expense. The model was further simplified based on the fact that maize stalk failure typically occurs above the node [17]. This means that it was unnecessary to simulate material that is below the stalk node. Therefore, simulations only modeled above the node, across the yz plane; these models were called quarter models. Fig. 2.6 summarizes the geometry simplifications applied to each stalk geometry.

[17] Robertson *et al.*, "Maize Stalk Lodging: Flexural Stiffness Predicts Strength," 2016.

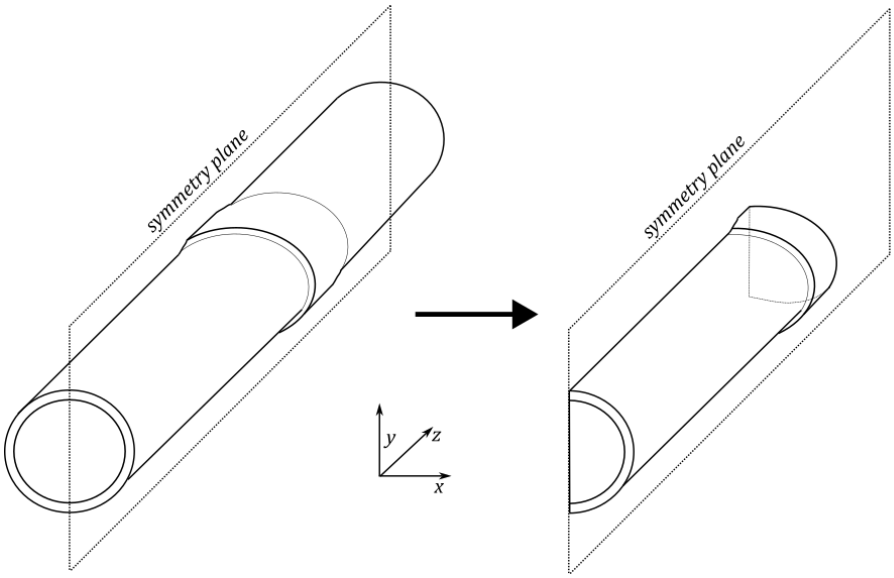

Figure 2.6: Simplifications to stalk geometry.

2.2.7 Subroutine 7: Mesh

The mesh used for each stalk consisted of two parts: a C3D4 (quadratic) tetrahedral region and a C3D8 hexahedral region. Fig. 2.7 shows the layout of the mesh applied to each model geometry.

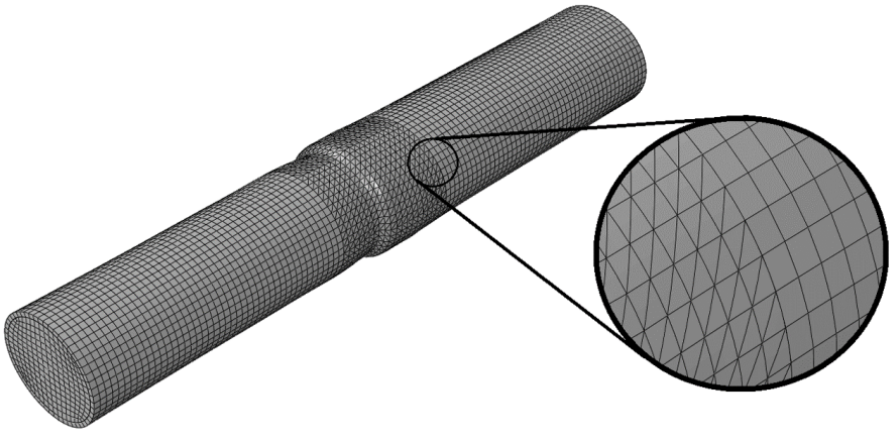

Figure 2.7: Mesh regions in maize stalk models, from Ottesen [18].

In general, tetrahedral (tet) elements have more weaknesses than hexahedral (hex) elements, and hex elements should be used whenever possible [22]. Tet elements were used in the node region due to significant geometric variation that hex elements cannot accurately capture. Hex elements were used in the internode section of the geometry.

The mesh density was adjusted by assigning specific edges a designated number of elements, calculated as a multiple of a model mesh

[22] Benzley *et al.*, "A Comparison of All Hexagonal and All Tetrahedral Finite Element Meshes for Elastic and Elasto-plastic Analysis," 1995.

index parameter stored in inputs.py. Increasing the model mesh index parameter enhances the mesh density along each feature edge. A custom multiplier for each feature edge was determined iteratively. For simplicity, this thesis does not detail the specific number of elements along each feature edge.

2.2.8 Subroutine 8: Analysis and Post Processing

The final subroutine ran a user-selected analysis and then post-processed the results of the analysis. Subroutine 8 was therefore composed of three 'mini subroutines' that all work toward the goal of running analysis and interpreting results: 1) running the chosen analysis, 2) flex post processing, and 3) buckling post processing. If the user chose to run a flex analysis, then only functions 1) and 2) were used; if the user chose to run a buckling analysis, then only functions 1) and 3) were used.

Running the Chosen Analysis

Two different analyses could be performed on stalk geometries: linear static analysis and linear buckling analysis. These analyses were chosen because they most accurately capture the behavior observed from two different tests performed on physical maize stalks: flexural stiffness and failure strength. Physical testing was performed in three point bending configuration [13, 19].

Flexural stiffness refers to how stiff a stalk is; it describes how much force a stalk exerts when bent in the linear elastic region (when failure or nonlinearities are not present). This behavior can be replicated in FEA by applying a small load on a stalk and calculating its deflection. For small loads, a linear static (Newton) finite element solver is suitable for this situation.

[13] Al-Zube *et al.*, "The elastic modulus for maize stems," 2018.

[19] Al-Zube *et al.*, "Measuring the compressive modulus of elasticity of pith-filled plant stems," 2017.

Failure strength refers to the maximum applied force on a stalk before it fails. A linear eigenvalue (buckling) solver was used to calculate the maximum load before failure for stalks in three point bending. A linear eigenvalue solver operates by slowly scaling input loads until instability occurs. As such, the solver does not take into consideration any dynamic effects or material failure in the analysis. In spite of this, linear buckling analysis has been a commonly accepted and validated approach for calculating failure strength in maize stalk models [9, 10, 18].

Subroutine 8 therefore ran either a flexural stiffness (linear static) or a failure strength (linear buckling) analysis depending on which analysis the user chose. This was as simple as defining a keyword (either 'flex' or 'buckle') to Abaqus to start the solver.

[9] Ottesen *et al.*, "A parameterised model of maize stem cross sectional morphology," 2022.

[10] Stubbs *et al.*, "Maize stalk stiffness and strength are primarily determined by morphological factors," 2022.

[18] Ottesen *et al.*, "Development and stochastic validation of a parameterized model of maize stalk flexure and buckling," 2023.

Flex Post Processing

The results of a linear static analysis were deflections caused by the applied loads. The flexural stiffness, EI, has been used in previous studies as a predictor of stalk strength [17, 18]. Deflection was used with Castigliano's theorem to calculate EI. Castigliano's theorem is shown in Eqs. (2.1) to (2.3).

$$\delta = \frac{\partial}{\partial F} U \tag{2.1}$$

$$U = \int \frac{M^2}{2EI} dx \tag{2.2}$$

$$\delta = \int \frac{\partial M}{\partial F} \frac{M}{EI} dx \tag{2.3}$$

Flexural stiffness was then calculated using equations from Table 2.2 (see Eqs. (2.4) and (2.5)). Subroutine 8 performed these calculations on calculated deflections and returned the flexural stiffness to the user in CSV format.

$$\delta_a = \frac{1}{2} \int_0^a \frac{2M_a + Px}{EI} dx \tag{2.4}$$

$$EI_a = \frac{1}{\delta_a} \left(\frac{M_a a^2}{2} + \frac{Pa^3}{3} \right) \tag{2.5}$$

Buckling Post Processing

Linear buckling analysis produced eigenvalues and corresponding eigenvectors. The eigenvalues are scale factors; multiplying the user-defined applied load (see Table 2.2) by a buckling eigenvalue corresponds to the load required to cause structural instability. The eigenvectors are the shape of the instabilities (sometimes called a mode).

During linear buckling analysis, there was a chance that a computed failure strength corresponded to a buckling shape that was unrealistic. Fig. 2.8 illustrates common shapes that are unrealistic, such as ones influenced by mesh node locking or boundary effects.

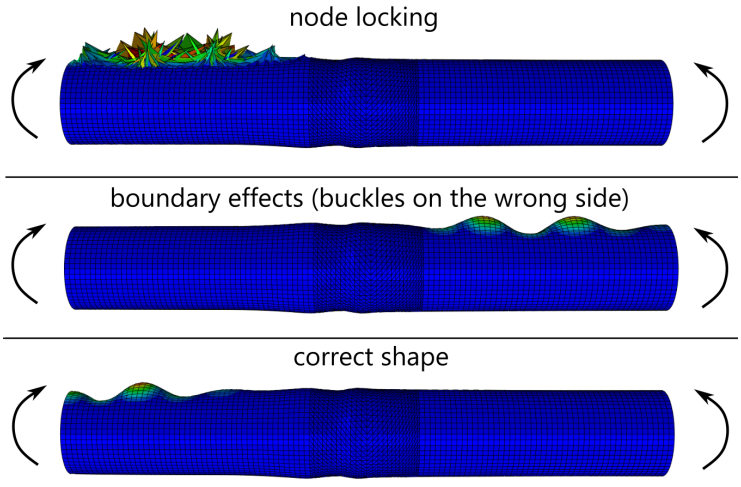

Figure 2.8: Examples of node locking, boundary effects, and correct modes from linear buckling analysis.

To classify the computed buckling nodes, a method was developed to check a computed shape for inaccuracies. This involved (1) exporting the buckling shape as a set of four contour lines, (2) determining which contour line captures the buckling shape, and (3) calculating the number of peaks and valleys of the contour line of interest (see Fig. 2.9). This caught buckling shapes calculated below the node and shapes affected by mesh node locking (shapes with more than 20 peaks and valleys). Subroutine 8 returned the eigenmode, eigenvector, and number of peaks and valleys to the user in CSV format. A minimum of three buckling shapes were calculated for each failure strength analysis with the knowledge that some computed shapes would be unrealistic.

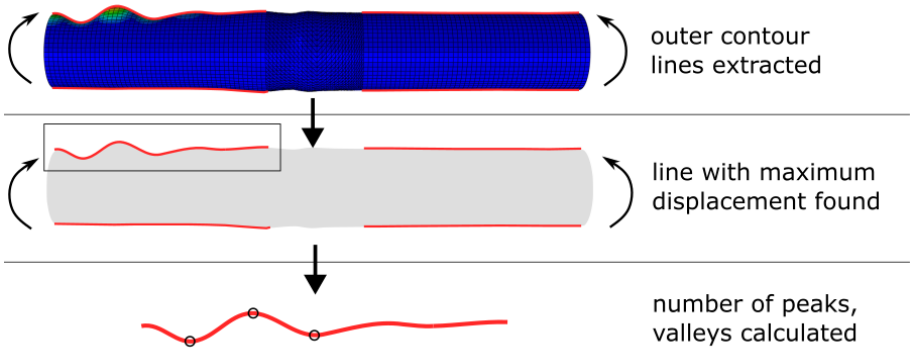

Figure 2.9: Post processing linear buckling results.

2.2.9 Subroutine Summary

The culmination of the eight subroutines described above is an automated package capable of generating and analyzing 3D parameterized maize stalk models. This method significantly reduces processing time compared to CT-based methods and facilitates in-depth studies on geometric sensitivity, as detailed in Chapter 4.

2.3 System Validation

2.3.1 Comparison of Quarter Symmetric Models to Whole Models

To verify that quarter symmetry simplifications did not significantly influence the predictive accuracy of our models, simulations were conducted on twenty stalk geometries using the quarter model simplification and compared to simulations of the full geometry. The results from both sets of models showed a high correlation, with an r^2 statistic of over 0.99 for both flexural stiffness and failure strength analyses.

2.3.2 Mesh Convergence

An important aspect of FEA meshing is the mesh convergence study [23]. This involves increasing mesh density at discrete intervals to evaluate the mesh's influence on results. For our geometries, a mesh convergence study was performed on both the pith and rind geometries by varying the model mesh index parameter.

[23] Hughes, *The Finite Element Method*, 1987.

The mesh convergence study consisted of increasing the model mesh index parameter in steps of 0.5. For pith convergence, the rind was kept at a fine model mesh index of 7 and the pith model mesh index was slowly increased from a coarse mesh of 1. The reverse was true for rind convergence. Fig. 2.10 shows the mesh convergence of the pith and rind geometries for both flexural stiffness analysis and linear buckling analysis. Convergence tests were conducted for both whole and quarter geometries, with nearly identical results. As seen in Fig. 2.10, an adequate model mesh index for both pith and rind meshes was a mesh index parameter of 3. Summary statistics for the number of elements used in the pith and rind regions, as well as the type of element with a model mesh index of 3, are provided in Section 2.4.

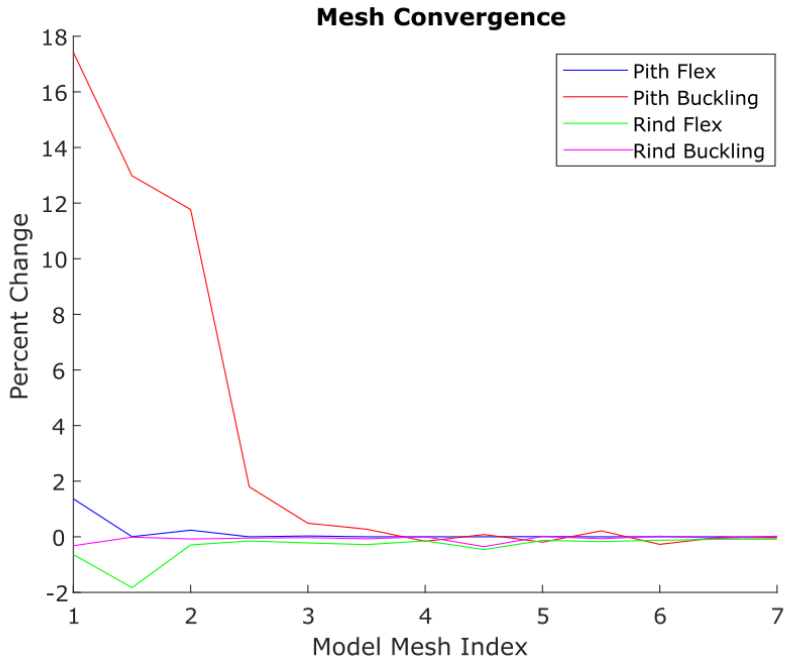

Figure 2.10: Mesh convergence. The model mesh index represents the relative degree of how fine the mesh is; 1 is a coarse mesh and 7 is a fine mesh. The y-axis shows the percent change from the last calculated result. For example, a percent change of 17 for pith buckling convergence at a model mesh index of 1 means the calculated buckling result at a model mesh index of 1 was 17% higher than the same result calculated at a model mesh index of 0.5. After a model mesh index of 3, the percent change between subsequent indices was less than 1%.

2.3.3 Validation Results

To validate the automation system, 63 maize stalks were generated and analyzed using Abaqus 2022, incorporating the methodologies outlined in the previous sections. Flexural stiffness (flex) and failure strength (buckling) test results were compared with physical testing results. As described in Section 2.2.3, variance was introduced to account for material uncertainties. The test results are shown in Figs. 2.11 and 2.12.

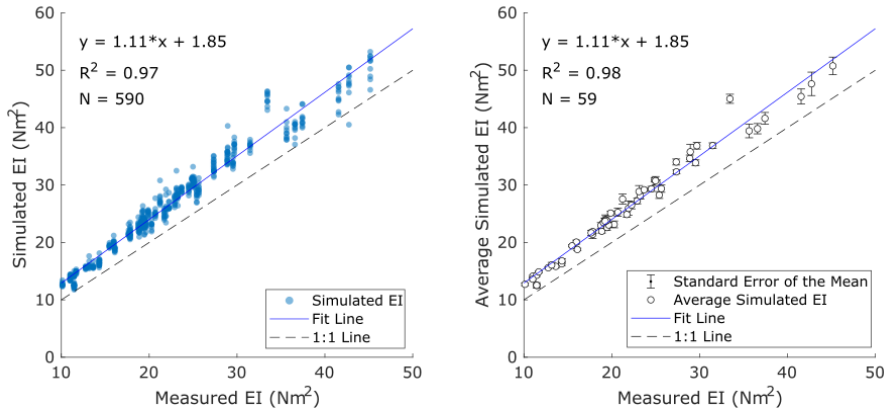

Figure 2.11: Whole geometry material variance and validation for flexural stiffness, from Ottesen [18].

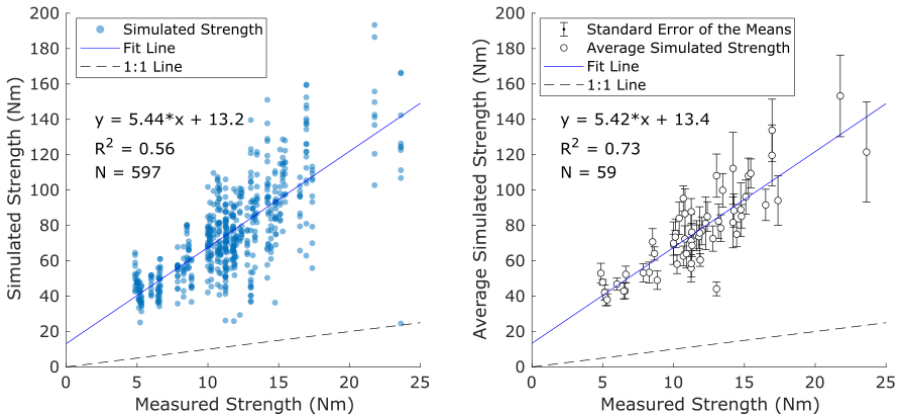

Figure 2.12: Whole geometry material variance and validation for failure strength, from Ottesen [18].

The 3D parameterized maize stalk model demonstrated strong correlations between model predictions and actual maize stalk behavior, particularly in flexural stiffness calculations. The strength of the relationship was not as strong for failure strength calculations, but still predictive of stalk strength. Buckling analyses are more sensitive to material constants as a result of the more complex mechanics of buckling. This issue is discussed further in Chapter 4.

2.4 Assessment of Automation System Performance

While model creation would typically require manual execution by an experienced finite element analyst, the automated package demonstrated in this chapter drastically reduces setup time. Manual execution typically takes at least 20 minutes per analysis, whereas the automated package presented here completes the same tasks in just seconds. Table 2.3 summarizes the mean model generation time for both whole and quarter models, for models with a model seed index of 3 (see Section 2.3.2). These statistics were gathered by generating 20 models of each case (20 quarter models, and 20 whole models). The 20 models were chosen through failure strength stratified sampling of the original 900 CT scanned stalks.

Table 2.3: Mean model generation time for whole and quarter models, in seconds.

	Whole	**Quarter**	**Whole / Quarter**
Model Generation Time	15 s	9 s	1.67

Table 2.4 shows the mean analysis runtime of these same generated models for both flex and buckling simulations. Quarter models run roughly twice as fast for flex simulations and nearly six times as fast for buckling simulations, while providing virtually identical results.

Table 2.4: Mean runtime for flex/buckling models for whole/quarter models, in seconds.

	Whole	**Quarter**	**Whole / Quarter**
Flex	47 s	25 s	1.88
Buckling	471 s	81 s	5.81

Table 2.5 shows the average and standard deviation number of elements present in both whole and quarter models for both pith and rind regions for each element type. This data was taken from the same 20 models described previously.

Table 2.5: Mean/standard deviation number of elements in each region by element type, also in percent form.

Element	**Whole Models**		**Quarter Models**	
	mean (std)	**%**	**mean (std)**	**%**
tet (rind)	38207 (6817)	44.09% (7.87%)	0 (0)	0.00% (0.00%)
hex (rind)	10752 (0)	12.41% (0.00%)	2800 (0)	16.43% (0.00%)
wedge (rind)	0 (0)	0.00% (0.00%)	600 (118)	3.52% (0.69%)
tet (pith)	13310 (746)	15.36% (0.86%)	6140 (911)	36.03% (5.35%)
hex (pith)	24384 (1160)	28.14% (1.34%)	7500 (0)	44.01% (0.00%)
wedge (pith)	0 (0)	0.00% (0.00%)	0 (0)	0.00% (0.00%)

Note that wedge elements were specifically used to replace tetrahedral elements in the rind region for quarter models. This was only feasible for quarter models, and was done because wedge elements perform slightly better than tet elements. The use of wedge elements only slightly affected convergence results in Section 2.3.2, which was performed for both whole and quarter models with similar results.

For hexahedral element regions, the standard deviation for both pith and rind meshes was zero (except for whole model pith hex elements, which were minimal), indicating consistent meshing regardless of geometry. In contrast, tetrahedral and wedge element regions showed non-zero standard deviations for both pith and rind meshes, reflecting some numerical noise associated with geometric changes in those regions.

2.5 Discussion

The results of the work in this chapter is a fully automated package capable of analyzing any 3D parameterized maize stalk geometry. This allows for researchers to more freely explore model behavior in sensitivity studies. The automated nature of this package facilitates rapid analysis of arbitrary model shapes, significantly enhancing efficiency in computational studies.

Validation results depicted in Figs. 2.11 and 2.12 demonstrate the predictive capability of the automated package. This makes the model a reliable tool for future investigations into maize stalk mechanics and behavior. It is estimated that over 50,000 simulations have been run using this automated package over the past 3 years.

The outcomes of this chapter lays a solid foundation for subsequent chapters, where the automated package will play a pivotal role in parameter sensitivity analysis. This automated package can also be used in future studies involving optimization of geometric parameters.

3 *Material Constant Measurement: Longitudinal Shear Modulus*

This chapter is composed from a paper entitled "Measurement of Maize Stalk Shear Moduli" published in the journal *Plant Methods* [25]. I hereby confirm that the use of this article is compliant with all publishing agreements.

[25] Carter *et al.*, "Measurement of Maize Stalk Shear Moduli," 2023.

3.1 Background

The material behavior of maize stalks is complex and important to capture in FEA models. As stated in Chapter 2, both pith and rind tissue are modeled as transverse isotropic materials. This means that many material constants are required in order to fully define their behavior. Many of these material constants have not yet been reported in literature. The purpose of this chapter was to measure the longitudinal shear modulus of rind and pith tissues. This will allow the resulting FEA models to be based upon measurements instead of estimates.

The mechanical behavior of transversely isotropic materials are determined by six material constants. Five of these material constants are independent [26]. When analyzing maize stalks (which are composed of two transversely isotropic materials), twelve (ten independent) material constants are needed to model their behavior. Because of the difficulties in measuring maize stalk tissues materials (e.g. asymmetrical geometry and variation in specimens), research on maize stalk material constants has been relatively limited.

[26] Boresi *et al.*, *Advanced Mechanics of Materials*, 2002.

Although data regarding maize stalk properties are scarce, some of the twelve material properties have been measured previously. The longitudinal modulus of rind tissue is the most commonly reported maize tissue property [13–15, 19]. This is because the longitudinal rind modulus is relatively simple to measure and it has been shown to be influential in failure modeling [9].

[13] Al-Zube *et al.*, "The elastic modulus for maize stems," 2018.

[14] Zhang *et al.*, "Tensile Properties of Maize Stalk Rind," 2016.

[15] Zhang *et al.*, "Mechanical Behavior of Corn Stalk Pith: an Experimental and Modeling Study," 2017.

[19] Al-Zube *et al.*, "Measuring the compressive modulus of elasticity of pith-filled plant stems," 2017.

[9] Ottesen *et al.*, "A parameterised model of maize stem cross sectional morphology," 2022.

The longitudinal modulus of pith tissue is more difficult to measure due to its low stiffness and fragility. Studies often adopt an inference-based approach to measure this property–a researcher will measure material response of an intact specimen (pith and rind), remove the pith, test the specimen again (with just the rind), and infer the contribution of the pith. Sutherland [16], Zhang [15], and Al-Zube [19] have reported the longitudinal modulus of elasticity of pith tissues.

[16] Sutherland *et al.*, "The Influence of Water Content on the Longitudinal Modulus of Elasticity of Maize Stalk Tissues," 2022.

[15] Zhang *et al.*, "Mechanical Behavior of Corn Stalk Pith: an Experimental and Modeling Study," 2017.

[19] Al-Zube *et al.*, "Measuring the compressive modulus of elasticity of pith-filled plant stems," 2017.

The transverse modulus of pith and rind tissue is also difficult to measure. This is because there are no closed form equations to calculate modulus values for transverse compression testing (as opposed to three point bending or simple tension testing). Stubbs used an inverse-FEA process in order to calculate the transverse modulus of elasticity of maize pith and rind tissues [10, 27].

For late-season stalk lodging, researchers are most interested in tissue properties at the time of harvest when stalks often have a relatively low moisture content. As a result, tissues are often classified as "dry" (moisture content below 15%) or "wet" (moisture content above 15%). Dry tissues are most relevant to late-season stalk lodging [28] while wet tissue properties are more relevant to mid-season stalk lodging or greensnap [16]. Dry tissues have the advantage of being more amenable to laboratory testing since they are much more stable and easier to test than wet tissues. In general, tissue stiffness is highest for dry tissues and decreases as moisture content increases [14–16].

While many properties have been measured, several remain unmeasured. The properties that have not yet been measured include poisson's ratios and shear modulus values. These properties are either difficult to measure or are believed to have a less significant influence on material response in maize stalks [9]. Of these remaining material properties, the longitudinal shear modulus of pith and rind tissue is the easiest to measure. This is because shear modulus is most often measured through torsion testing, and it is relatively easy to grip a maize stalk along its fibers (in the longitudinal direction). Table 3.1 summarizes the maize stalk tissue properties that have and have not been measured and shows how this chapter fills a gap in our understanding of maize stalk tissue properties.

[10] Stubbs *et al.*, "Maize stalk stiffness and strength are primarily determined by morphological factors," 2022.

[27] Stubbs *et al.*, "Measuring the transverse Young's modulus of maize rind and pith tissues," 2019.

[28] Robertson *et al.*, "On Measuring the Bending Strength Of Septate Grass Stems," 2015.

[16] Sutherland *et al.*, "The Influence of Water Content on the Longitudinal Modulus of Elasticity of Maize Stalk Tissues," 2022.

[14] Zhang *et al.*, "Tensile Properties of Maize Stalk Rind," 2016.

[15] Zhang *et al.*, "Mechanical Behavior of Corn Stalk Pith: an Experimental and Modeling Study," 2017.

[16] Sutherland *et al.*, "The Influence of Water Content on the Longitudinal Modulus of Elasticity of Maize Stalk Tissues," 2022.

[9] Ottesen *et al.*, "A parameterised model of maize stem cross sectional morphology," 2022.

Table 3.1: Summary of which maize stalk tissue properties have and have not been measured, including whether measurements were included for both wet and dry specimens.

Source	$E_{\|\|}$	$E_{\perp}$	$G_{\|\|}$	$G_{\perp}$	$\nu_{\|\|}$	$\nu_{\perp}$	**Pith**	**Rind**	**Wet**	**Dry**
Al-Zube [19]	✓							✓		✓
Al-Zube [13]	✓							✓		✓
Stubbs [27]		✓					✓	✓		✓
Stubbs [29]		✓					✓	✓		✓
Sutherland [16]	✓						✓	✓	✓	✓
Zhang [14]	✓							✓	✓	✓
Zhang [15]	✓						✓		✓	✓
This chapter			✓				✓	✓		✓

The goal of this research was to measure the longitudinal shear modulus of dried maize stalk pith and rind tissues so that future studies that require these properties can be based upon empirical data instead of estimates, as has been necessary in the past [9, 18, 29]. In particular, measurements were taken only on dried maize stalk samples for two reasons: first, dried stalks are easier to measure than wet ones; and second, because researchers are most concerned with stalk behavior at the time of harvest, when stalks are relatively dry [16, 28, 29]. Through this research, a 95% confidence level distribution of pith and rind longitudinal shear moduli was developed. This knowledge will be used to improve computational models of maize stalks, thereby enabling a better understanding of the mechanisms involved in stalk lodging.

[9] Ottesen *et al.*, "A parameterised model of maize stem cross sectional morphology," 2022.

[18] Ottesen *et al.*, "Development and stochastic validation of a parameterized model of maize stalk flexure and buckling," 2023.

[29] Stubbs *et al.*, "Mapping spatially distributed material properties in finite element models of plant tissue using computed tomography," 2020.

3.2 Methods

Torsion tests were performed on dried maize stalks by twisting specimens (see Fig. 3.1). Specimens were gripped at the node to prevent crushing due to the gripping pressure. The applied torque and rotation were measured simultaneously during each test. Following each test, the geometry of the stalk was quantified. Finally, the shear modulus was calculated based on the torque/rotation slope and the geometry of the specimen.

[16] Sutherland *et al.*, "The Influence of Water Content on the Longitudinal Modulus of Elasticity of Maize Stalk Tissues," 2022.

[28] Robertson *et al.*, "On Measuring the Bending Strength Of Septate Grass Stems," 2015.

[29] Stubbs *et al.*, "Mapping spatially distributed material properties in finite element models of plant tissue using computed tomography," 2020.

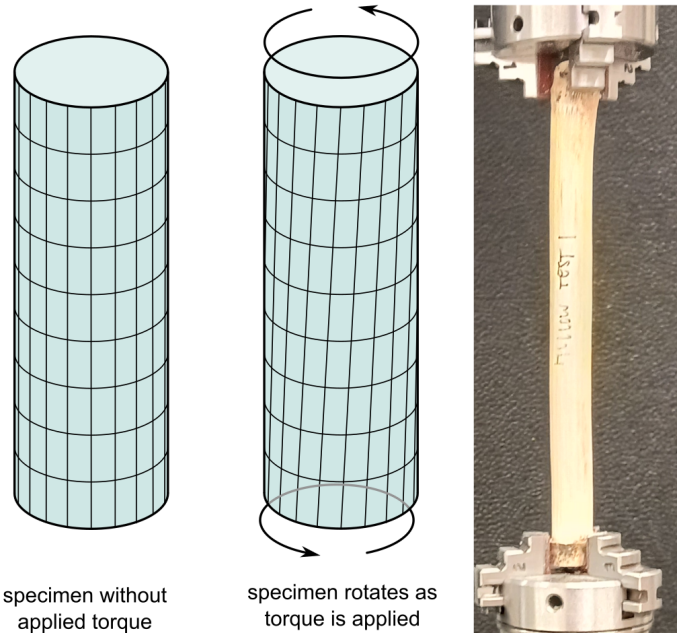

Figure 3.1: Torsion testing illustration and photograph of experimental set up.

The general approach used in this chapter is similar to well established methods for measuring similar materials [30]. Such torsion tests were conducted on dried bamboo [31–33] and 10-12% moisture content wood [21, 34].

[30] *ASTM E143-20: Standard Test Method for Shear Modulus at Room Temperature*.

[31] Revelo *et al.*, "Development of a Method to Test Bamboo Culms in Direct Torsion," 2022.

[32] Askarinejad *et al.*, "Effects of humidity on shear behavior of bamboo," 2015.

[33] Moran *et al.*, "A new method to measure the axial and shear moduli of bamboo," 2017.

[21] Green *et al.*, *Wood Handbook: wood as an engineering material*, 1999.

[34] Brabec *et al.*, "Utilization of digital image correlation in determining of both longitudinal shear moduli of wood at single torsion test," 2016.

3.2.1 Theory

The shear modulus, G is a measure of a material's resistance to shear deformation. For a prismatic 3D member, the equation relating shear deformation θ to applied torque T is:

$$\theta = \frac{TL}{GK} \tag{3.1}$$

Here L represents the length over which the torque is applied and K is the torsional constant, a factor that accounts for the cross-sectional geometry of the object [35]. This equation can be solved for the shear modulus:

[35] Budynas *et al.*, *Roark's Formulas for Stress and Strain*, 2020.

$$G = \frac{T}{\theta}\frac{L}{K} \tag{3.2}$$

For a circular section, this simplifies to the more familiar form $\frac{TL}{J\theta}$ where J is the polar area moment of inertia. However, for a specimen of arbitrary cross section (as for a maize stalk), the torsional constant should be used [26, 36].

The theory described above relies upon several assumptions. First, the theory assumes that the member subjected to torsion is prismatic. Second, the theory assumes that the tissue is linearly elastic with small levels of deformation. These assumptions are discussed below.

[26] Boresi *et al.*, *Advanced Mechanics of Materials*, 2002.

[36] Popov *et al.*, *Mechanics of Materials*, 2015.

"Prismatic" means that the cross section of a specimen is uniform along its length. While the cross-sectional shape of maize stalks is not perfectly uniform, there is very little change in the cross-sectional shape between nodes [28]. The nearly uniform shape of the maize stalk is shown in Fig. 3.2.

[28] Robertson *et al.*, "On Measuring the Bending Strength Of Septate Grass Stems," 2015.

The assumption for small deformations in Eqs. (3.1) and (3.2) are met so long as the angle of twist is small. To account for this, specimens were twisted only a small amount: from 0 to 5 degrees. This approach kept measurements within the linear elastic region.

3.2.2 Specimen Groups and Selection

Specimens came from maize stalks that were grown in an open field in Spanish Fork Utah during the 2021-2022 growing seasons. Three different commercial varieties of maize were used for testing. However, since the purpose of this chapter was to report a range of feasible values for the longitudinal shear modulus of maize, the influence of variety was not used as an experimental factor. Stalks were harvested once grain filling had completed and just before harvest. This time point corresponds to the period when late-season stalk lodging is most likely to occur [28]. The stalks were cut with pruning shears just above the root and immediately transferred to the lab for specimen preparation. Fig. 3.2 shows a representative sample cutting location on an intact maize stalk.

[28] Robertson *et al.*, "On Measuring the Bending Strength Of Septate Grass Stems," 2015.

Specimen dimensions were limited by the physical constraints of the torsion tester (MTS Acumen 12, Eden Prairie, MN). The maximum length of specimens was constrained to 20 cm and the maximum diameter of

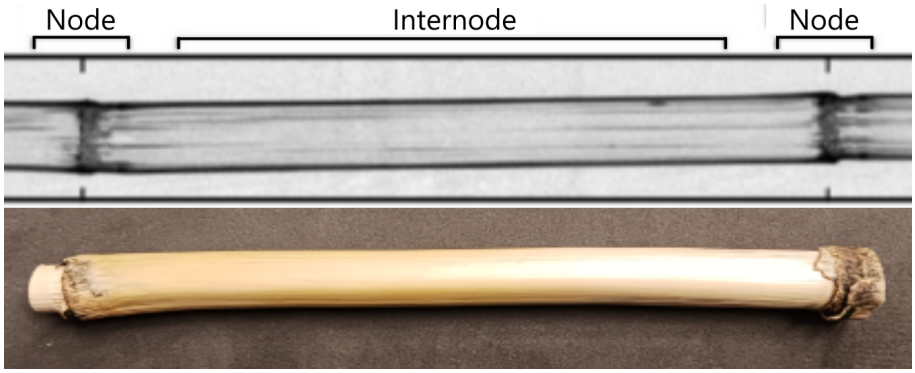

Figure 3.2: Example specimen location for sample selection. The specific location of a stalk was chosen based on whether the length was less than 20 cm and the diameter was less than 2.5 cm.

specimens was constrained to 2.5 cm. These limits excluded only a small number of very large diameter stalks. Cuts were made 2-3 centimeters above and below a node (see Fig. 3.2) so that miniature lathe chucks could grip the nodes, which are sturdier and easier to grip. Each specimen was inspected for disease, pest damage, cracks, or any other damage before being chosen. Any damaged specimens were excluded from testing.

Two different specimen groups were created in order to observe specific phenomena in testing: rind-only specimens (pith tissue removed), and pith-only specimens (rind tissue removed):

Rind Only Specimens: Specimens with only rind tissue were used to directly measure the shear modulus of the rind. To create rind-only specimens, the pith was carefully removed using drill bits, dissection spatulas, and abrasive pipe cleaners. Care was taken to ensure that the rind was not damaged in this process. If cracking occurred during pith removal, the specimen was not used. Due to the difficulty in preparing rind-only specimens, only 18 rind-only tests were performed.

Pith Only Specimens: Specimens with only pith tissue were used to directly measure the shear modulus of the pith. To create pith-only specimens, the rind was carefully removed using a razor blade. If cracking occurred during rind removal, the specimen was not used.

3.2.3 Gripping Specimens

Gripping specimens is always a challenge with biological tissues. If specimens are not gripped tightly enough, slipping may occur which adversely affects the collected data. On the other hand, if specimens are gripped too tightly, the specimen may be damaged. To mitigate these problems, 180 grit sandpaper was glued to the gripping jaws. This allowed the jaws to provide substantial gripping force which prevented slipping while also avoiding crushing or cracking the specimen. Tests were not performed if cracks occurred during the grip tightening phase.

Because gripping involves multiple points of contact, the center of rotation can change slightly depending on how a specimen is gripped. To mitigate this effect and to account for other sources of random measurement errors, each specimen was fixtured and tested using 3-5 replications of the torsion test.

Standard Torque/Angle Measurement

Both torque T and angle of twist θ were measured by a 3 kip-MTS Acumen torsion/tensile testing device. The torque transducer for this device was a 662.30H-02B Model 30 N m capacity transducer. The angle measurement for this device was a 494.47 Encoder B Rotary Encoder. Each specimen was loaded from 0 to 5 degrees at a rate of 0.15 degrees per second. This load speed was chosen because it was deemed slow enough to be considered static loading (viscoelastic effects could be neglected). Torque and angle were measured simultaneously during testing.

Assessing Slippage: Alternative Angle Measurement

As stated previously, any shifting/slipping of the specimen during the torsion test will produce inaccuracies in the angle of twist measurement. Slipping can occur incrementally, making it very difficult to detect. To assess whether or not slippage of the grips was a problem, a second method for measuring the angle of twist was developed. This second method relied upon the rotation of two lasers attached directly to the specimen itself (see Fig. 3.3). Because there are no external loads applied to the lasers, this approach is not subject to any slippage. Under the laser method, two Feyachi 9 mm bore sight lasers were attached at the outer thirds of each specimen as shown in Fig. 3.3. The lasers were aimed at a grid located a known distance from the specimen. A Nikon DSLR Z2 camera with a zoom lens was used to capture the location of the laser dots relative to the grid. During torsion testing, the lasers twisted with the maize stalks, and the paths of the laser dots were captured by a sequence of photographs.

To align the laser data with the torque and rotation data, the Nikon camera was triggered using an output signal from the torsion tester. Two photographs were taken every second during a torsion test (2 Hz sampling). As most tests took approximately 2 minutes to complete, this resulted in over 200 photographs per test. Each frame captured by the camera was analyzed using computer vision techniques to determine the position of each laser dot over time. Using trigonometry, the angle of twist between the two points was calculated over time, as shown in Fig. 3.3.

Comparing Encoder Rotation with Laser Rotation

Rotation was thus measured using two approaches: the rotations of the grips themselves as recorded by the rotary encoder (we call this the 'rotary encoder' measurement procedure), and the rotation as measured by the laser method described above (we call this the 'laser' measurement procedure). Any discrepancies between the two tests provided evidence

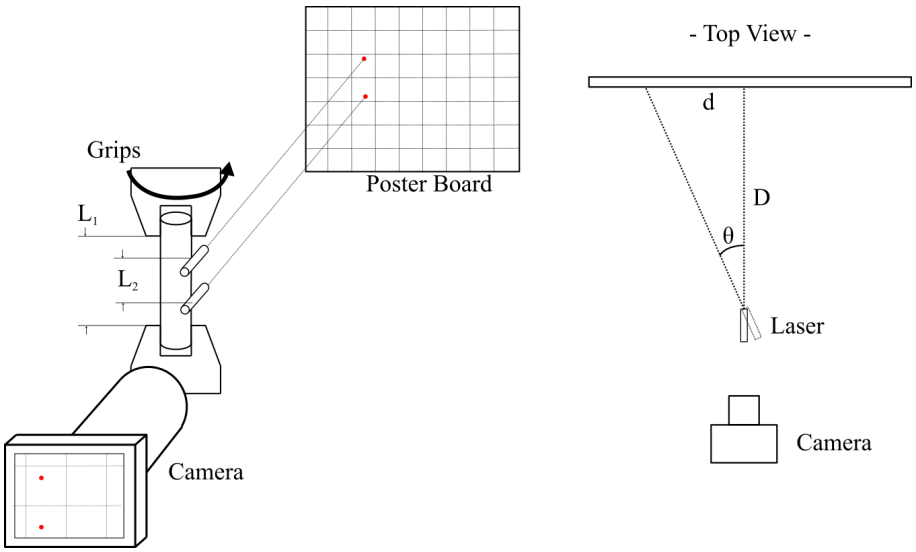

Figure 3.3: Laser setup. Left: two lasers were attached to the outer thirds of a specimen and pointed at a grid-poster board some distance away. A camera with a zoom lens tracked the movement of the laser dots over time. L_1 was the grip length used in the torsional stiffness calculation for standard samples, and L_2 was the grip length used in the torsional stiffness calculation for laser samples. Right: Trigonometry of camera setup. The angle was calculated with $\theta = tan^{-1}[d/D]$, where d was the position of the laser dot on the poster board and D was the distance from the laser to the poster board.

of slippage. Because the length of specimen differed between grips and between lasers, the appropriate quantity for comparison between the rotary encoder data and the laser data was the torsional stiffness, GK, which is defined as:

$$GK = \frac{T}{\theta}L \tag{3.3}$$

Where T was the torque measured by the MTS Acumen (identical in both tests); was the angle of twist; and L was the length of the specimen for which twist was measured. These lengths are shown in Fig. 3.3 as L_1 (for the standard measurement) and L_2 for the laser measurement. A two sample t-test was used to compare results obtained using this laser measurement technique and those measured using the 'standard' angle measurement technique. Comparisons between the two methods for measuring rotation are presented in Section 3.3.1.

3.2.4 Quantifying Specimen Geometry

Specimen Length Measurements

The effective length L of each specimen was measured. Before a torsion test began, a standard 1 mm precision flexible tape measure was used to measure the distance between the grips. This distance measurement was used for each subsequent test per specimen. Uncertainties in length measurements are explored in Section 3.2.5.

Specimen Cross-sectional Geometry

Formulas from *Roark's Formulas for Stress and Strain* [35] were used to calculate K for both pith-only sections and rind-only sections. For pith-only cross sections, Roark's equation for arbitrary solid cross sections was used:

[35] Budynas *et al.*, *Roark's Formulas for Stress and Strain*, 2020.

$$K_{pith} = \frac{A_{pith}^2}{40 J_{pith}} \tag{3.4}$$

Where A_{pith} is the area encapsulated by the pith section and J_{pith} is the polar moment of the area of the pith section. For hollow rind-only cross sections, Roark's equation for arbitrary thin walled hollow cross sections was used:

$$K_{rind} = \frac{4A_m^2}{\oint ds/t} \tag{3.5}$$

Here A_m was the area encapsulated by the thin wall midline, s was the distance along the midline, and t was a function of s along the midline. The geometric information used in these equations was obtained from optical scans of specimen cross sections. Specimens were first cut perpendicular to their length with a bandsaw to expose the inner cross-section. These cross sections were held against an Epson Perfection V39 flatbed scanner and scanned at 2400 dpi. These images were then exported to Matlab (MathWorks, Natick, MA) as JPEGs for image processing.

In Matlab, the Visual Processing Toolbox's `imageSegmenter` function was used to create digital masks of each image. A region of interest tool was used to mark the relevant pixels for calculations. Fig. 3.4 outlines various steps of this process.

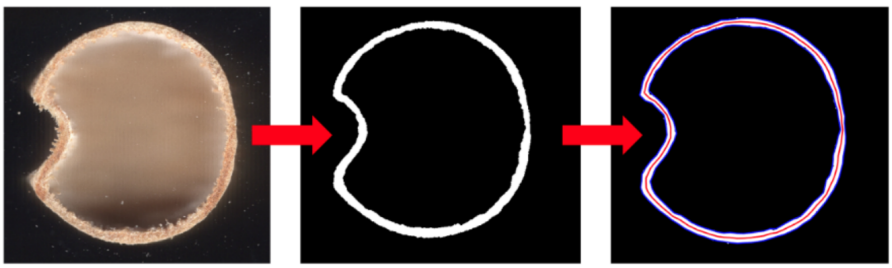

Figure 3.4: Three steps of the image segmentation process. We first imported an image to Matlab (left), then we separated the rind pixels from the pith pixels using the segmenter tool (middle), then relevant quantities were calculated using Matlab functions (right).

3.2.5 Uncertainty in Measurements

It is important to consider the degree of uncertainty when reporting measured values of plant tissues [37]. Three quantities were required to calculate shear modulus: the T/θ slope, L, and K. Each of these

[37] Nelson *et al.*, "Measurement accuracy and uncertainty in plant biomechanics." 2019.

quantities were subject to measurement uncertainty. In this chapter, we will define the measurement uncertainty of all quantities as the two-sided 95% confidence interval of the mean measurement. This quantity is written as

$$u = t_{95,n-1}\frac{s}{\sqrt{n}} \tag{3.6}$$

Where $t_{95,n-1}$ was the 95% confidence t-statistic drawn from the student's t distribution with $n-1$ degrees of freedom, s was the sample standard deviation, and n was the number of measurements for a given specimen.

The quantity T/θ was measured 3 to 5 times for each specimen with the MTS Acumen. The specimen was removed from the machine and refixtured between each test. The standard deviation of these measurements was used in Eq. (3.6) to calculate $u_{T/\theta}$ for each set of repeated specimen measurements. This uncertainty was unique for each specimen.

The quantity L was measured as the distance between the two grips for a specimen. This was measured with a standard 1mm increment tape measure. To estimate the variation in measuring the length L, one sample was fixtured and measured 10 times by one user. The standard deviation of this repeated measurement was used with Eq. (3.6) to calculate an uncertainty that was applied to all samples.

The quantity K was measured through numerical integration of the formulas described in Section 3.2.4. The biggest source of error in this measurement came from variation in manually identifying the pixels in a cross section scan as being either pith pixels or rind pixels. Erroneously identifying pith pixels as being rind pixels would inflate the K calculated for the rind while depressing the K value for the pith. To estimate the variation caused by the manual segmentation process, the torsional constant of one cross section scan was calculated 10 times by one user. The standard deviation of the resulting torsional constants was used with Eq. (3.6) to calculate a u_K that was applied to both pith-only and rind-only specimens.

Propagation of Uncertainty

The Monte Carlo error propagation method [38] was used to determine the overall uncertainty in shear modulus. The mean and standard deviation values for T/θ, L, and K were calculated for each specimen. Normal distributions were then created for each quantity based on these respective mean and standard deviations. These distributions were then sampled 100 times for each quantity and combined to produce a distribution of corresponding G values. The mean G value was carried forward as the best estimate of G for each specimen. The standard deviation of the G distribution was used with Eq. (3.6) to calculate the propagated uncertainty in shear modulus, u_G.

[38] Coleman *et al.*, *Experimentation, Validation, and Uncertainty Analysis for Engineers*, 2009.

It is often easier to visualize uncertainties in terms of percent uncertainty. The percent uncertainty for any of the quantities discussed above can be calculated with Eq. (3.7):

$$u_{\%} = (u/\bar{X}) \times 100\% \tag{3.7}$$

Where u was the uncertainty calculated in Eq. (3.6) and $\bar{X}$ was the mean measured value for a specimen. Because $\bar{X}$ was unique for each specimen, the percent uncertainty varied for each specimen. In Section 3.3.3, we will report the 95% confidence intervals on the uncertainties found for T/θ, L, K, and G.

3.3 Results

3.3.1 Influence of Slippage

The paired t-test between the standard measurement method and the laser measurement method showed that there was no significant difference between the two methods (p-value of 0.2846). As seen in Fig. 3.5, the medians of the two measurement distributions are virtually identical. Because slipping is not possible when using the laser method, and because there was no difference in data between the laser method and the standard methods, we concluded that slippage was negligible when using the grips approach. As a result, subsequent test results are not differentiated by the method used in measuring rotation.

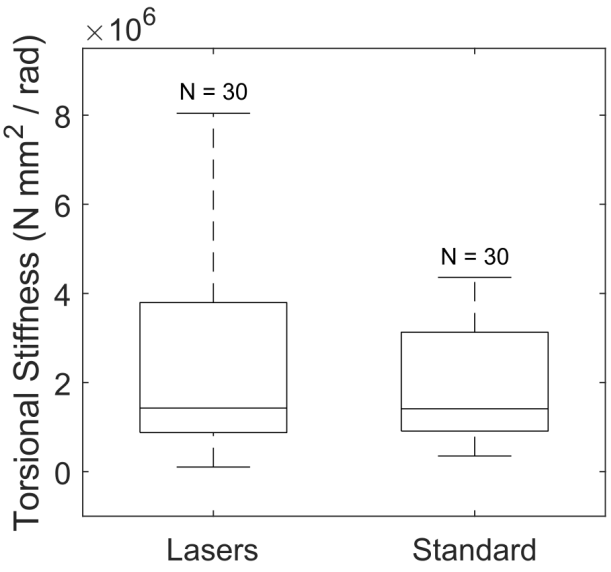

Figure 3.5: Torsional stiffness calculated using laser-based angle measurements ("Laser") and the standard MTS method ("Standard").

3.3.2 Shear Modulus Distributions for Rind and Pith Tissues

Rind shear moduli measurements varied from 355 MPa to 1630 MPa and had an approximately normal distribution with a mean of 931 MPa and standard deviation of 334 MPa. Pith shear moduli measurements varied from 13 MPa to 55 MPa and had an approximately normal distribution with a mean of 27 MPa and standard deviation of 10 MPa. The coefficients of variation for these distributions were very similar, 36% for the rind, and 37% for the pith. Fig. 3.6 shows the measured distributions for pith and rind tissues.

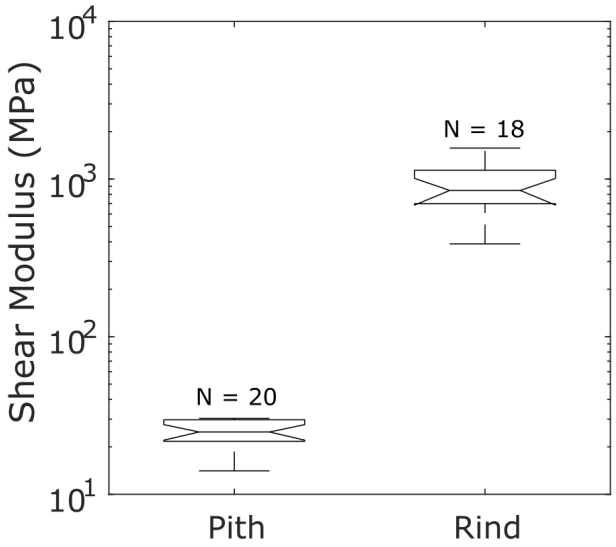

Figure 3.6: Measured pith and rind shear moduli.

Comparison to Similar Materials

Wood and bamboo are relatively similar to maize and can be used as comparison. Moran [33] reported the mean shear modulus of Guadua Angustifolia (dry) bamboo to be 638 MPa. Green [21] reported the mean shear modulus of hard woods to be 768 MPa, and soft woods to be 692 MPa. The measured rind shear modulus was found to be slightly higher than these averages, with a mean of 931 MPa.

[33] Moran *et al.*, "A new method to measure the axial and shear moduli of bamboo," 2017.

[21] Green *et al.*, *Wood Handbook: wood as an engineering material*, 1999.

Fig. 3.7 shows that the measured rind values fall within both Green and Moran's ranges for wood and bamboo. As expected, the measured shear modulus values for pith were significantly lower than the other tissues. This is because pith tissue has a density far lower than those materials.

3.3.3 Measurement Uncertainty

The 95% percent confidence interval of propagated uncertainty for shear modulus was between 5.9% and 13.44% for rind samples. The 95% percent confidence interval of propagated uncertainty for shear modulus was between 5.77% and 7.17% for pith samples. The largest source

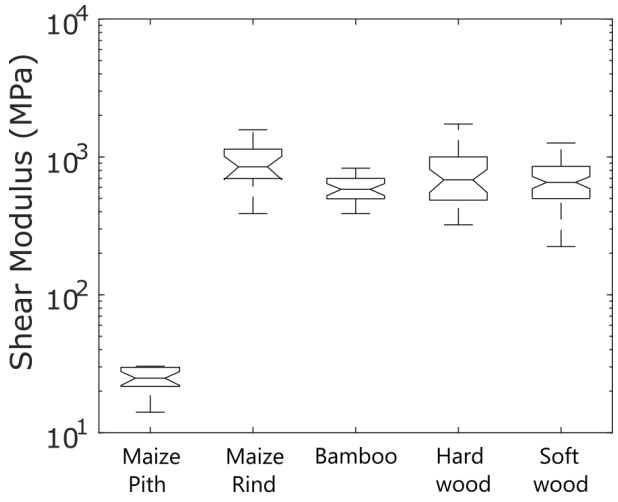

Figure 3.7: Comparison between measured shear modulus values for dry (< 15% moisture) specimens of maize pith, maize rind, bamboo, hardwood and softwood. Bamboo values are from Moran [33], wood values are from Green [21].

for this error came from uncertainties in slope ($u_{T/\theta}$). 95% confidence intervals for measurement uncertainties are shown in Table 3.2. Because these uncertainties are relatively small, they were not included in the results shown in Figs. 3.6 and 3.7.

Table 3.2: 95% confidence intervals for measurement uncertainties in slope, length, torsional constant, and measurement of shear modulus.

	$u_{T/\theta}$	u_L	u_K	u_G
Rind	3.12% - 4.83%	0.66% - 0.88%	0.35% - 0.86%	4.36% - 12.5%
Pith	4.16% - 12.8%	0.94% - 1.17%	0.11% - 0.16%	3.18% - 4.75%

3.4 Discussion

There are several reasons for confidence in the measured shear modulus values. Firstly, tested specimens did not slip due to applied torque. This is because t-testing showed that measurement techniques impervious to specimen slipping produced the same results as standard techniques. This means that the data is not biased towards the effects of specimen slipping.

Second, the measured values agree well with reported values for similar materials. The measured rind modulus fell within the same ranges for wood and bamboo, which are relatively similar to corn tissue. As expected, the measured pith values were much lower than rind values, as has been reported elsewhere for maize tissues [10, 16].

[10] Stubbs *et al.*, "Maize stalk stiffness and strength are primarily determined by morphological factors," 2022.

[16] Sutherland *et al.*, "The Influence of Water Content on the Longitudinal Modulus of Elasticity of Maize Stalk Tissues," 2022.

Lastly, the measurement uncertainties were similar to those reported for several methods for measuring the longitudinal stiffness of maize tissues in a prior study [13]. The majority of this error came from variability in repeated specimen testing. Similar phenomena have been seen in previous studies and are common in biological material, so this error is understandable.

The results of the measurements in this chapter were used in the analysis in Chapter 4, and will be used in future studies involving 3D parameterized maize stalk models. This allows us to better model the material behavior of maize stalks, and is an important piece in understanding stalk lodging.

[13] Al-Zube *et al.*, "The elastic modulus for maize stems," 2018.

3.5 Limitations

All specimens came from maize stalks having a relatively low moisture content, (10-15% moisture by weight). An inverse relationship between moisture content and tissue stiffness has been reported in several previous studies of plant tissues [16, 21, 39, 40]. As a result, lower modulus values are to be expected for tissues with higher moisture content.

Several factors such as axial variation, the influence of moisture content, tissue maturity, and other factors were beyond the scope of this chapter. Axial variation of tissue bending strength, flexural stiffness, and the influence of the leaf sheath have all been shown to vary along the axial length of the stalk [41–43]. Shear modulus also likely varies with axial position but was not investigated. Moisture content is known to affect the mechanical properties of maize tissues [14, 16]. In addition, the behavior of immature tissues, diseased tissues, and "goosenecked" stalks have been observed (qualitatively) by the authors to differ significantly from those of mature tissues. As a preliminary study on the longitudinal shear modulus of maize stalk tissues, this chapter focused on dry tissues and did not investigate the issues of axial variation, tissue maturity, disease, or goosenecking.

[16] Sutherland *et al.*, "The Influence of Water Content on the Longitudinal Modulus of Elasticity of Maize Stalk Tissues," 2022.

[21] Green *et al.*, *Wood Handbook: wood as an engineering material*, 1999.

[39] Zabler *et al.*, "Moisture changes in the plant cell wall force cellulose crystallites to deform," 2010.

[40] Rowell *et al.*, *The Chemistry of Solid Wood; Advances in Chemistry*, 1984.

[41] Oduntan *et al.*, "The effect of structural bending properties versus material bending properties on maize stalk lodging." 2024.

[42] Martin-Nelson *et al.*, "Axial variation in flexural stiffness of plant stem segments: measurement methods and the influence of measurement uncertainty," 2021.

[43] Hale *et al.*, "Assessing axial and temporal effects of the leaf sheath on the flexural stiffness of large-grain stems." 2023.

[14] Zhang *et al.*, "Tensile Properties of Maize Stalk Rind," 2016.

[16] Sutherland *et al.*, "The Influence of Water Content on the Longitudinal Modulus of Elasticity of Maize Stalk Tissues," 2022.

4 Sensitivity Analysis of 3D Parameterized Models

4.1 Background

Research has suggested that the shape of maize stalks can greatly influence their ability to withstand stalk lodging [7, 8, 10]. However, these studies relied primarily upon an observational approach. This approach was used in prior studies to identify correlational patterns between gross morphological features and stalk strength. To gain a more nuanced understanding and establish causation, direct modification of the stalk geometry is required. In actual practice, direct modification of the structural attributes of the maize stalk is extremely difficult. A promising alternative is to use sophisticated computational models which allow precise control over each aspect of the maize stalk. The 3D parameterized maize stalk model developed previously provides direct control over individual geometric and material features of the maize stalk [18]. This type of model enables studies such as sensitivity analyses and optimization studies to shed more light on the mechanics of stalk strength and failure.

[7] Von Forell *et al.*, "Preventing lodging in bioenergy crops: a biomechanical analysis of maize stalks suggests a new approach," 2015.

[8] Robertson *et al.*, "Maize Stalk Lodging: Morphological Determinants of Stalk Strength," 2017.

[10] Stubbs *et al.*, "Maize stalk stiffness and strength are primarily determined by morphological factors," 2022.

[18] Ottesen *et al.*, "Development and stochastic validation of a parameterized model of maize stalk flexure and buckling," 2023.

A sensitivity analysis is a powerful tool that can be used to characterize the manner in which features of a system influence its behavior [44]. This is done by changing each aspect of the model on a one-at-a-time basis to determine what impact this change has on the model output [45]. Sensitivity analysis has been used to study growth and development in the field of agronomy, including wheat [46], potatoes [47], and rice [48].

[44] Saltelli *et al.*, *Sensitivity Analysis*, 2009.

[45] Hamby, "A Comparison Of Sensitivity Analysis Techniques," 1995.

[46] Richter *et al.*, "Sensitivity analysis for a complex crop model applied to Durum wheat in the Mediterranean," 2010.

[47] Gao *et al.*, "Image processing-aided FEA for monitoring dynamic response of potato tubers to impact loading," 2018.

[48] Confalonieri *et al.*, "Comparison of sensitivity analysis techniques: A case study with the rice model WARM," 2010.

The purpose of this chapter is to understand how geometric and material properties of maize stalk models influence maize stalk flexural stiffness, failure strength, and biomass. This will be done using a sensitivity analysis combined with statistical data from actual experiments. These results will enable researchers to better understand how geometric and tissue parameters of the maize stalk contribute to the behaviors listed above. This understanding can help guide future efforts to mitigate stalk lodging via selective breeding or genetic manipulation.

4.2 Methods

4.2.1 Overview

Sensitivities in this paper were computed using the 3D parameterized maize stalk model that was described in previous chapters. Rather than modeling the entire stalk, this model captures the failure region: the

region immediately apical of the node [49]. The model approximates each cross-section of an individual maize stalk using two ellipses, one for the outer boundary and one for the rind/pith boundary. Axial variation is captured by allowing the elliptical cross-section to vary along the length of the stalk. One advantage of this model is that it can be used to efficiently create specimen-specific models from experimental data. An original specimen-specific model and a corresponding parameterized model are shown in Fig. 4.1. The colored paths on the parameterized model illustrate the major diameter, minor diameter, and rind thickness paths that define the elliptical cross-sections of the model at each axial location.

[49] Robertson *et al.*, "Corn Stalk Lodging: A Forensic Engineering Approach Provides Insights into Failure Patterns and Mechanisms," 2015.

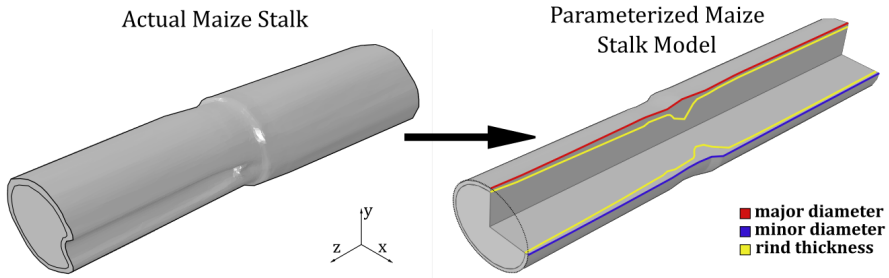

Figure 4.1: The parameterized maize stalk model. The highlighted lines are the inner and outer exterior edges of the rind geometry. The outer edges are simply the major and minor diameter landmark paths, and the inner edges are the major and minor diameter landmark paths with the rind thickness feature path subtracted.

The 3D parameterized maize stalk model is defined by a number of geometric parameters as well as a set of material tissue parameters. This model was used to perform a comprehensive sensitivity analysis to determine how the parameters that define the model influence the flexibility, strength, and total biomass.

4.2.2 Sensitivity Analysis

Sensitivity S is essentially a partial derivative that quantifies the influence of factor X_i on response Y_j:

$$S_{ij} = \frac{\partial Y_j}{\partial X_i} \tag{4.1}$$

Sensitivities are frequently normalized by reference values to obtain a non-dimensionalized form of sensitivity, S^*_{ij}:

$$S^*_{ij} = \frac{\partial Y_j}{\partial X_i} \frac{X_{i,ref}}{Y_{j,ref}} \tag{4.2}$$

Here $X_{i,ref}$ is the reference value of factor X_i, which is a material or geometric input parameter, and $Y_{j,ref}$ is the corresponding response when all X_i factors are at their reference values. The structural characteristics of interest were flexural stiffness, failure strength and biomass. The

non-dimensional form allows comparison across inputs that may have different units. We can discretize either of these equations using a finite difference approach:

$$S^*_{ij} = \frac{Y_{j,new} - Y_{j,ref}}{X_{i,new} - X_{i,ref}} \frac{X_{i,ref}}{Y_{j,ref}} \tag{4.3}$$

Where the subscript "new" refers to a quantity calculated with a modified input factor.

4.2.3 Refined Parameterization

The original parameterization approach [18] utilized 51 geometric parameters. Of these 51 parameters, 36 were used to define geometric landmarks (12 parameters per path) and 15 were used to define the transition patterns between landmarks (5 per path). While this parameterization adequately captured the overall shape of the maize stalk and provided good predictive accuracy, we found that this parameterization approach did not offer the level of control required for a sensitivity study. This is because changes to a single landmark tended to influence the shape of the model on both sides of the modified landmark. To provide more localized control over the stalk geometry, we introduced additional control points between landmarks. Fig. 4.2 illustrates both the original and updated parameterization schemes.

[18] Ottesen *et al.*, "Development and stochastic validation of a parameterized model of maize stalk flexure and buckling," 2023.

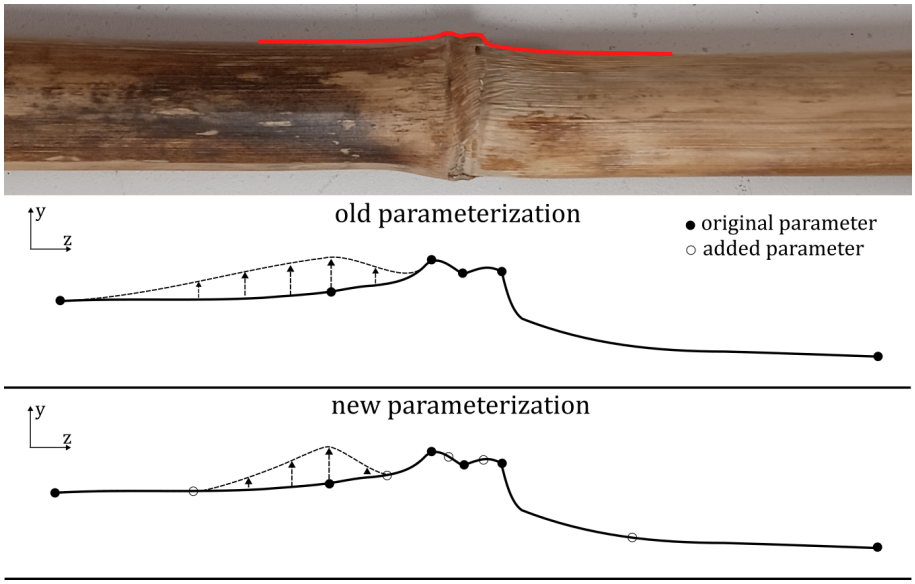

Figure 4.2: The parameterized path for major/minor stalk diameter as a function of axial position. Top Panel: Photograph showing the major diameter path traced in red. Middle Panel: The original parameterization of the major diameter. Bottom Panel: The updated parameterization with additional control points (open circles) located at the point of maximum discursion of the transition pattern between landmark points (closed circles). As seen by comparison between the two panels, changes to a landmark in the updated parameterization scheme have a more limited influence than in the original scheme. Note: The changes shown here have been exaggerated for illustrative purposes.

These new parameter points provided a much greater level of control over geometric features while still preserving the characteristics of the original parameterization technique. A validation study confirmed that models with 96 parameters provided identical results to corresponding models with 51 parameters.

Parameterization Challenges

The new parameterization allowed for very fine control of geometric parameters to influence stalk shape. However, it presented some new challenges to the sensitivity analysis.

First, although the parameterization provided fine control over geometry, changing just one geometric parameter by a small amount resulted in an extremely small change in overall model shape. The model's finite element mesh has been optimized to accurately capture overall model response, but does not accurately capture these small changes. A mesh convergence could have been performed for each parameter modified in this chapter. This would have required 96 mesh convergence studies. Another alternative would have been to create a single mesh that was sufficiently detailed that it could capture any minor change in the stalk geometry. Either of these approaches would have required thousands of hours of manual modeling and computational effort. In addition, the resulting mesh(es) would have required many hundreds or thousands of additional computing time to perform the sensitivity analysis. The resulting change in stiffness or strength was therefore sometimes difficult to detect in the presence of some degree of "noise" which is due to the computational mesh. Levels of modification that were large enough to detect clearly often resulted in model geometries that were highly distorted.

Secondly, after fitting the parameterized model to 900 individual maize stalks, we discovered that most model parameters are not truly independent, but instead are highly correlated with neighboring parameters. Traditional one-at-a-time sensitivity analysis entirely neglects correlations between model parameters, resulting in sensitivities that could be misleading [50].

These challenges were addressed using a statistical technique called principal component analysis (also known as empirical eigenfunction analysis). Principal component analysis captures and describes natural patterns of variation observed in a data set. In our case, these patterns involved coordinated variation patterns involving the 96 model parameters.

[50] Groen *et al.*, "Ignoring correlation in uncertainty and sensitivity analysis in life cycle assessment: what is the risk?" 2017.

Principal Component Analysis

Principal component analysis transforms a dataset into a new coordinate system defined by empirical basis "functions" that capture the largest variation in the data [51]. These functions, known as principal components, serve as the foundation of the data. The first principal component captures the most variation, while subsequent components capture progressively less.

[51] Jackson, *A User's Guide to Principal Components*, 1991.

Principal component analysis can be used to reduce the dimensionality of a system because the ranking of the principal components can be used to 'cut off' information which can be neglected or omitted with a minimal loss of fidelity. For example, in a model with 100 parameters (or dimensions), if the first three principal components account for 95% of the variation, we could use only these three principal components and achieve a very similar set of behaviors using just 3 dimensions instead of the original 100 dimensions. This machine learning technique has been used in many fields, often dealing with morphology, including complex drawing assemblies [52], and structural components [53].

Because principal component analysis is a statistical technique that uses variations in model parameters, it also preserves any existing relationships between model parameters [54]. This means that we can use principal component analysis on our 96 geometric parameters and still preserve how model parameters move according to nature. In the sections below, we outline how principal components were calculated for our 96 geometric parameters.

[52] Schwarz *et al.*, "Principal component analysis and singular value decomposition used for a numerical sensitivity analysis of a complex drawn part," 2018.

[53] Xiao *et al.*, "On-the-fly model reduction for large-scale structural topology optimization using principal components analysis," 2020.

[54] Ramsey *et al.*, *The Statistical Sleuth: A Course in Methods of Data Analysis*, 2013.

Parameter Grouping Approach

A data set of 900 maize stalk geometries were fitted to the 3D parameterized model which has been used and described in previous studies [9, 10, 18]. The fitting approach produced a matrix of model parameters having 900 rows (one for each stalk) and 96 columns (the geometric parameters). Principal component analysis was performed on this data set. Prior to performing principal component analysis, each parameter was standardized according to Eq. (4.4):

[9] Ottesen *et al.*, "A parameterised model of maize stem cross sectional morphology," 2022.

[10] Stubbs *et al.*, "Maize stalk stiffness and strength are primarily determined by morphological factors," 2022.

[18] Ottesen *et al.*, "Development and stochastic validation of a parameterized model of maize stalk flexure and buckling," 2023.

$$X_{i,standardized} = \frac{X_i - \bar{X}_i}{s_{X_i}} \tag{4.4}$$

Where X_i are the original parameters, $\bar{X}_i$ is the mean parameter value and s_{X_i} is the standard deviation of the X_i values. Standardization was applied to remove scaling effects between parameters of different units. In addition, standardization ensured that each parameter exerted an equal influence on the total variance of the data set. Principal component analysis was performed using a pre-built function in Matlab 2022. The output of principal component analysis was a 96 by 96 matrix of principal components (called P), a 900 by 96 matrix of principal component coefficients (called C), and a vector of 96 eigenvalues that described the total variance explained by each principal component. The original fitted parameter matrix (X_{orig}) could be reconstructed with Eq. (4.5).

$$X_{orig} = CP^T s_X + \bar{X} \tag{4.5}$$

Where C is the coefficients matrix and P is the principal component matrix. In order to convert to the space of the original parameters, de-standardization was applied (multiplying by standard deviation and adding the mean in Eq. (4.5)).

The principal component approach essentially re-parameterized the maize stalk model. Instead of controlling the geometry through one-at-a-time variation of individual geometric parameters, the principal component approach allowed us to control the geometry by adjusting the amount of each principal component present in each model. Fig. 4.3 provides an example of what a +100% standard deviation change to the first principal component looks like for a representative stalk model. More information on the mechanics of this process is provided in further sections.

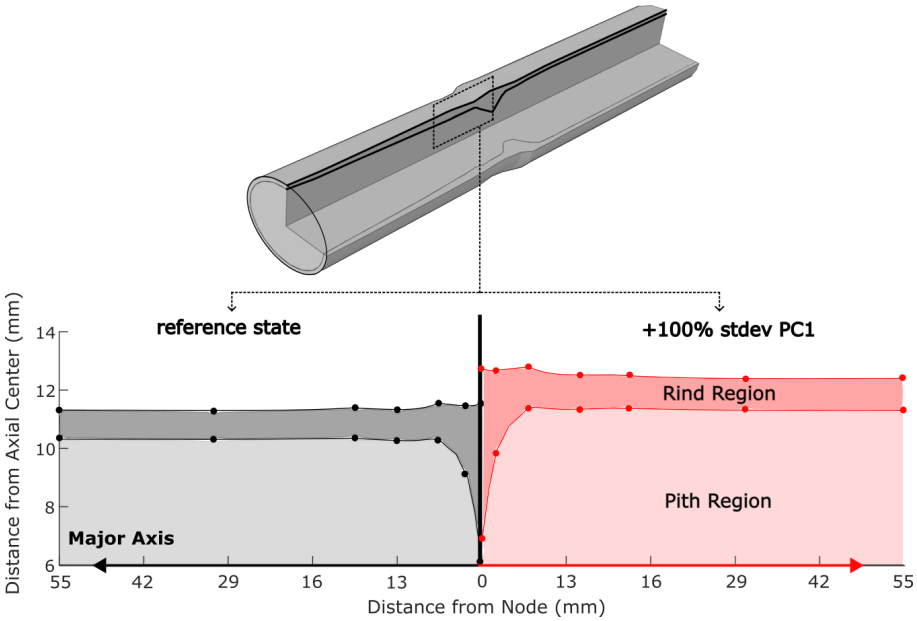

Figure 4.3: Visualizing the first principal component. The left side (in black) is the stalk at its 'reference' state (no changes to the principal component). The right side (in red) is the same stalk with a +100% standard deviation increase applied to the model's first principal component. Each stalk is mirrored across from each other in order to show the differences between the two (the only part of each stalk shown is the region above the node–regions below the node are not shown).

For sensitivity analysis, we treated the first twenty columns of principal component coefficients (from the matrix C) as the new control 'parameters' of the 3D parameterized model. Each entry in the matrix C represents the amount of a given principal component present in the model. By increasing a given column in the principal component coefficient matrix, we could 'twist a knob' that increased the amount of a given principal component.

4.2.4 Finite element models and analyses

The parameterization techniques outlined in Section 4.2.3 were used to generate 3D parameterized stalk models using SolidWorks. These 3D CAD models were then imported into the commercial finite element software Abaqus for structural analysis. The results of finite element analysis were used to calculate sensitivities.

Analyses Performed

Two mechanical responses of the 3D parameterized maize stalk model were investigated: flexural stiffness and failure strength. Flexural stiffness was calculated using a linear static analysis. Failure strength was calculated using linear buckling analysis. Details on the loading conditions for both cases are provided in Section 4.2.4.

Material Properties

As in previous studies [9, 10], we modeled the maize stalk rind and pith tissues using a transversely isotropic elastic material model. A transversely isotropic material consists of six material constants, five of which are independent [55]. Fig. 4.4 provides a diagram depicting these six material properties.

[9] Ottesen *et al.*, "A parameterised model of maize stem cross sectional morphology," 2022.

[10] Stubbs *et al.*, "Maize stalk stiffness and strength are primarily determined by morphological factors," 2022.

[55] Milton, *The Theory of Composites*, 2002.

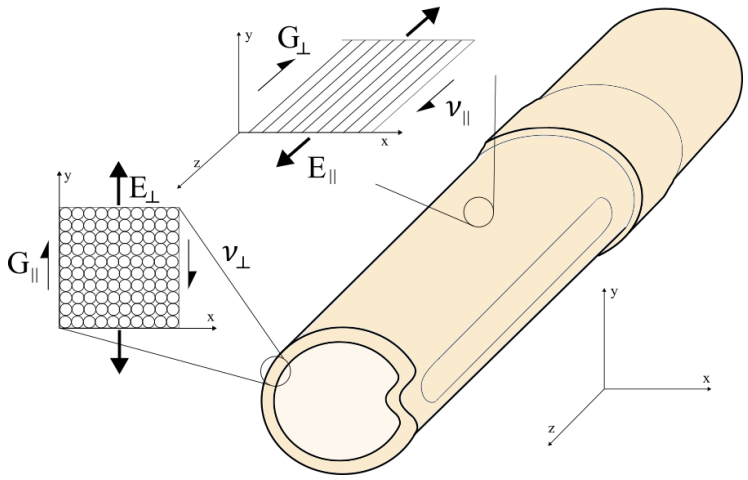

Figure 4.4: Interpretation of transverse isotropy material constants. The || symbol indicates a property in the fiber direction, while the ⊥ symbol indicates a property perpendicular to the fibers. Material direction is highlighted for the rind tissue, but this orientation is also present in pith tissue.

There were twelve different material constants required to define the material response of maize stalks, ten of which were independent. The ranges that were used in this chapter for each of these material constants are shown in Table 4.1 along with the sources for each range.

Boundary Conditions

Because the parameterized maize stalk model has an elliptical cross-section, it has two symmetry planes. A symmetry boundary condition in the yz plane was used to simplify the model and reduce computational expense. The model was further simplified based on the fact that maize stalk failure typically occurs above the node [17]. This means that it is unnecessary to simulate material that is below the stalk node. Therefore, we only simulated the section above the node, with symmetry across the xy plane [56]; we called these models 'quarter models'. Fig. 4.5 summarizes the geometry simplifications applied to each 3D parameterized stalk geometry.

[17] Robertson *et al.*, "Maize Stalk Lodging: Flexural Stiffness Predicts Strength," 2016.

[56] Touzani, *Finite Elements and Symmetry*, 2020.

Table 4.1: Material constant ranges for maize stalk pith and rind tissue, from Ottesen [18]. Units in GPa.

property	method	distribution	pith	rind	source
$E_{\perp}$	random sampling	normal	(0.026, 0.01)	(0.85, 0.39)	Stubbs [10]
rind $E_{\|\|}$	specimen specific	empirical	n/a	specimen specific	Al-Zube [13]
pith $E_{\|\|}$	random sampling	normal	(0.45, 0.05)	n/a	Sutherland [16]
$G_{\perp}$	calculated	n/a	$\frac{E_{\perp}}{2(1+\nu)}$		theory
$G_{\|\|}$	random sampling	normal	(0.27, 0.01)	(0.93, 0.33)	Carter [25]
$\nu_{\perp}$	random sampling	uniform	(0.2, 0.45)		Green [21]
$\nu_{\|\|}$	random sampling	uniform	(0.009, 0.086)		

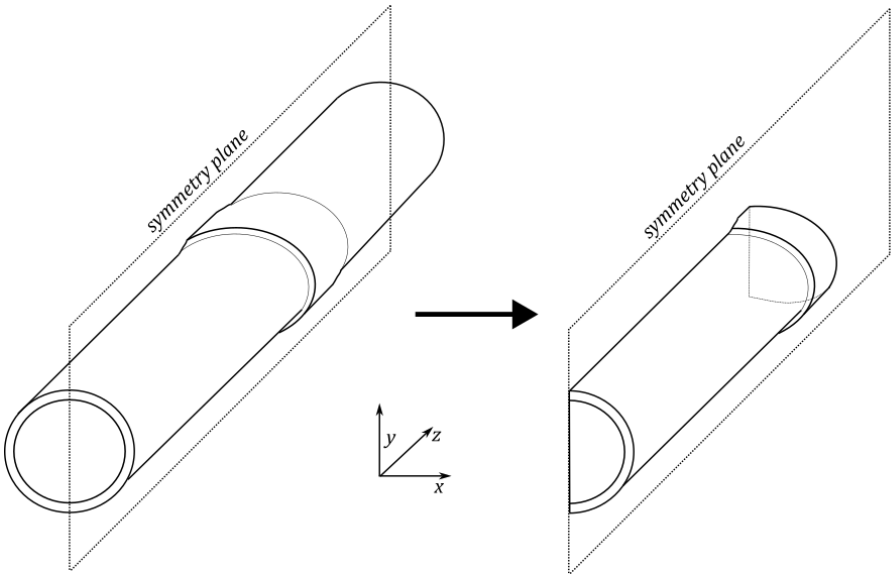

Figure 4.5: Simplifications to stalk geometry.

To verify that these simplifications did not significantly influence the predictive accuracy of our models, we simulated twenty stalk geometries using the 'quarter model' simplification and twenty geometries with the full geometry for comparison. The model results between these two groups correlated with each other with an r^2 statistic of over 0.99 for both flexural stiffness and failure strength analyses.

Cantilever bending loading boundary conditions were applied to all quarter-stalk models. In previous papers [18], we had used three point bending boundary conditions because validation data was based on physical three point bending tests. With the model fully validated, we used cantilever loading boundary conditions because these conditions more accurately match the loads experienced by maize stalks in real life [57].

[18] Ottesen *et al.*, "Development and stochastic validation of a parameterized model of maize stalk flexure and buckling," 2023.

[57] Kumar *et al.*, "Bending and Cutting Characteristics of Maize Stalk Residue," 2015.

To calculate flexural stiffness under cantilever loading, a linear static analysis was used. The static analysis consisted of applying simulated loads to calculate deflections. The simulated deflections were used to calculate the flexural stiffness of each model [18]. To calculate failure strength, linear buckling analysis was used. This type of analysis gradually applies larger and larger loads until instabilities occur in the model. The results of a linear buckling analysis are an eigenvector (the geometric shape of the instability) and an eigenvalue [58] (a scalar multiple for applied loads that will result in the corresponding instability). Multiplying this eigenvalue by the applied moment on a stalk gives the maximum moment before failure.

[18] Ottesen *et al.*, "Development and stochastic validation of a parameterized model of maize stalk flexure and buckling," 2023.

[58] Falzon *et al.*, *Buckling and Postbuckling Structures*, 2008.

Calculating Model Biomass

In addition to mechanical response, model biomass was calculated by multiplying the volume of pith/rind tissue by their respective densities. Pith and rind densities were based upon empirical measurements. These measurements were made using the samples from Chapter 3, which included measurements of cross sectional area and sample length. Densities were calculated by assuming prismatic specimens, calculating volumes with areas/lengths, and then weighing each sample to calculate density (density = mass/volume). This process was repeated for 20 pith samples and 20 rind samples.

The average density of pith samples was 83 kg/m^3 (standard deviation 27 kg/m^3) and the average density of rind samples was 810 kg/m^3 (standard deviation 280 kg/m^3). The measured mean density of rind samples has very similar densities to wood [59] and bamboo [60]. Because both pith and rind densities had such high variation (coefficients of variance each being roughly 0.3), both pith and rind densities were randomly sampled twenty times for each sensitivity calculation to account for uncertainties due to variations in density. This will be covered in Section 4.2.5.

[59] Saranpaa, *Wood Quality and its Biological Basis*, 2009.

[60] Huang *et al.*, "Density distribution profile for internodes and nodes of Phyllostachys edulis (Moso bamboo) by computer tomography scanning," 2015.

To calculate the sensitivity of models to biomass we used the sensitivity approach shown in Eq. (4.6).

$$S_{mass} = \frac{\partial m}{\partial X} = \frac{\partial V_{rind}\rho_{rind}}{\partial X}\frac{\partial V_{pith}\rho_{pith}}{\partial X} = \rho_{rind}\frac{\partial V_{rind}}{\partial X} + \rho_{pith}\frac{\partial V_{pith}}{\partial X} \quad (4.6)$$

Where X was a model input (in this case, a geometric parameter, as we did not calculate volume sensitivities for material properties in this chapter), m was the model mass, V was the model volume, and ρ was the tissue density.

Model volumes were estimated using numerical integration. The parameterization technique outlined in Section 4.2.3 resulted in major diameter, minor diameter, and rind thickness paths for each stalk model that had a user-defined number of points located between each of the geometric parameters. 100 points were defined between each landmark point. The volume of a particular stalk was calculated by calculating the area of an ellipse using the major and minor diameters at each user-defined point along these paths, and then integrating these areas along the axial length of a stalk model (trapezoidal integration). Fig. 4.6 visualizes the approach used to calculate volumes.

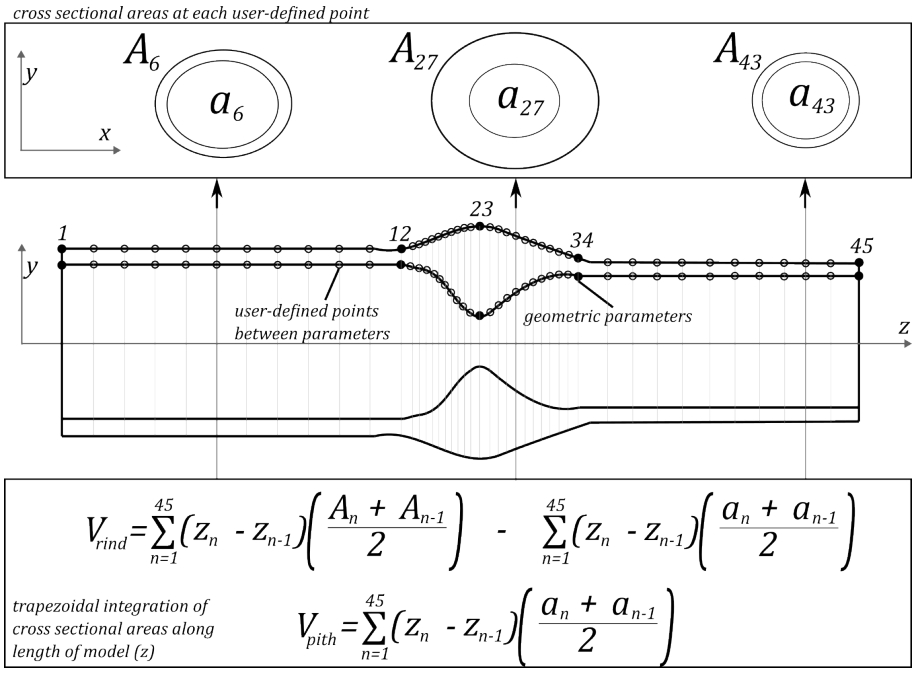

Figure 4.6: Approach used to calculate model volumes using trapezoidal integration. The 'A' symbol is the cross sectional area of both the pith and rind ellipse section together, and the 'a' symbol is the cross sectional area of just the pith ellipse section. To calculate just the volume of the rind, the total volume is subtracted from the pith volume.

4.2.5 Sampling Approach

The reference values for factors X and responses Y as explained in Eqs. (4.2) and (4.3) were calculated from 'base models'. We defined a 'base model' as one of the 900 specimen-specific parameterized geometries. Only a subset of these 900 parameterized geometries were chosen for use in sensitivity analysis through stratified sampling. Stratified sampling was used because it provides a more representative sample than simple random sampling [61]. The goal was to calculate 1000 unique values of sensitivities for both material and geometric sensitivities. Stratified sampling consisted of ordering all 900 parameterized geometries by stalk strength (measured from a previous study [13, 19]), and then choosing a specified number of 'base models' from linearly spaced indices.

[61] Särndal *et al.*, *Model Assisted Survey Sampling*, 2003.

[13] Al-Zube *et al.*, "The elastic modulus for maize stems," 2018.

[19] Al-Zube *et al.*, "Measuring the compressive modulus of elasticity of pith-filled plant stems," 2017.

Number of Material Sensitivity Calculations

Twenty 'base models' were selected for material sensitivity calculations. For each base model, each of the ten material constants were randomly sampled according to the distributions shown in Table 4.1. To account for variations in material constants, this process was repeated five times for each base model. With ten unique material properties (plus one case where the material properties were at their reference state), five material samplings, and twenty 'base models', the total number of simulations required to calculate the material sensitivities was:

20 geometries $\times$ 5 random samples $\times$ (1 reference case + 10 materials) = 1100 simulations = 1000 sensitivity values

Number of Geometric Sensitivity Calculations

Fifty 'base models' were selected for geometric sensitivity calculations. For each 'base model', each of the ten material constants were randomly sampled according to the distributions shown in Table 4.1. Contrary to material sensitivities, the material constants for each 'base geometry' were sampled only once. With fifty 'base models' and twenty principal components (plus one case where the 'base model' geometry was at its reference state), the total number of simulations required to calculate geometric sensitivities was:

50 geometries $\times$ (1 reference state + 20 principal components) = 1050 unique simulations = 1000 sensitivity values

Number of Geometric Mass Sensitivity Calculations

The estimated distributions for pith and rind densities as described in Section 4.2.4 had high coefficients of variance (roughly 0.3). Due to this high uncertainty, for geometric mass sensitivity calculations, we randomly sampled both the pith and rind densities twenty times for each sensitivity calculation. In all other ways, the sensitivity calculation setup was identical to those of Section 4.2.5, except repeated twenty times with

a different randomly sampled pith and rind density using the ranges in Section 4.2.4. This means a total of 20,000 sensitivities were calculated for geometric mass sensitivities.

In order to determine whether or not randomly sampling pith and rind densities had a significant impact on biomass sensitivity calculations, an error uncertainty was calculated for each sensitivity calculation. The error uncertainty was calculated with Eq. (4.7).

$$u = t_{95,n-1}\frac{s}{\sqrt{n}} \tag{4.7}$$

Where u was the uncertainty in the sensitivity, $t_{95,n-1}$ was the t-statistic, s was the standard deviation of the sensitivity as a result of variations in random samples for pith and rind densities, and n was the number of samples in the sensitivity distribution. In this case, $n = 20$ because the pith and rind densities were sampled twenty times for each sensitivity calculation.

4.2.6 Finite Difference for Sensitivity Calculations

We applied a percent standard deviation step size to X_{ref} for finite difference calculations. Taking percent standard deviation steps assures that all parameters are changed in proportional amounts. For material sensitivities, this was as simple as just adding 25% of a standard deviation to the material constant of interest. For geometric sensitivities, percent standard deviation changes were applied to the principal component coefficient matrix C (see Section 4.2.3). The principal component coefficient matrix was normalized prior to this so that standard deviations were evenly scaled. In turn, this required the principal component matrix to be scaled by the inverse of the normalization applied to C. Like material sensitivity calculations, a 25% standard deviation change was applied to the first twenty principal component coefficients for geometric sensitivity calculations.

4.2.7 Regression between Full and Reduced Parameterized Models

After geometric sensitivities were calculated, statistical analysis was performed to determine whether a 'reduced' model consisting of only the first principal component could be constructed to capture the majority of stalk behavior. This approach provided valuable insights into which principal components are most important for predicting stalk strength.

Twenty 'base geometries' were created using both the 'reduced' model setup (using only the first principal component) and the 'full' setup (using all principal components), and then analyzing these geometries for flexural stiffness, failure strength, and biomass. The data were then fit to a linear model and the r^2 value was used as the measure of correlative strength. A high r^2 meant that the 'reduced' model setup predicted the majority of flexural stiffness, failure strength, and biomass found using the 'full' model setup.

The number of principal components chosen to represent the 'reduced' model setup was determined by using the principal components that had the highest flexural stiffness, failure strength, and biomass normalized sensitivities. As will be explained in Section 4.3.2, there was only one principal component that was distinguishable from the rest. Therefore, only one principal component was used for the 'reduced' model setup.

4.2.8 Regression between Principal Components and Maize Stalk Behavior

A statistical analysis was performed to determine whether the principal components correlated with physical stalk behavior. This is important to do because if the principal components are not correlated with physical stalk behavior, then the 3D parameterized model has no connection to reality. It also provides insights into how principal components influence behaviors in actual maize stalks.

A previous study provided the failure strength and section moduli of each of the 900 tested stalks used to generate our principal components [13]. Another previous study provided the section moduli of these same 900 stalks [8]. We performed statistical analysis between these failure strengths, section moduli, and the principal component coefficients. Section modulus was considered in this analysis because Robertson found a high correlation between section modulus and failure strength in maize [8].

[13] Al-Zube *et al.*, "The elastic modulus for maize stems," 2018.

[8] Robertson *et al.*, "Maize Stalk Lodging: Morphological Determinants of Stalk Strength," 2017.

Least squares regression was used to calculate correlations between each set of data. This involved fitting a least squares polynomial to principal component, failure strength, and section modulus data. The r^2 statistics of the most parsimonious fitted polynomials were used to characterize the strength of relationship between principal components, failure strength, and section modulus for actual (not modeled) maize stalks [62]. Failure strength was considered over flexural stiffness and biomass because ultimately, it has a larger impact on stalk lodging than the other two.

[8] Robertson *et al.*, "Maize Stalk Lodging: Morphological Determinants of Stalk Strength," 2017.

[62] Navidi, *Statistics for Engineers and Scientists*, 2020.

4.3 Results

4.3.1 Material Sensitivity Results

Fig. 4.7 shows the ranked influence of material properties on flexural stiffness (i.e. sensitivity of flexural stiffness to material properties). The elastic modulus of rind tissue parallel to the fibers (rind $E_{||}$), was far more influential than any other material property. Shear modulus of pith and rind tissue parallel to the fibers (rind and pith $G_{||}$), as well as the rind Poisson's ratio parallel to the fibers (rind $\nu_{||}$) had median sensitivities less than 10%. All other material constants had sensitivities less than 1%. Distributions that were deemed statistically not significant (ns) from one sample t-testing ($p > 0.05$) are marked with an 'ns'.

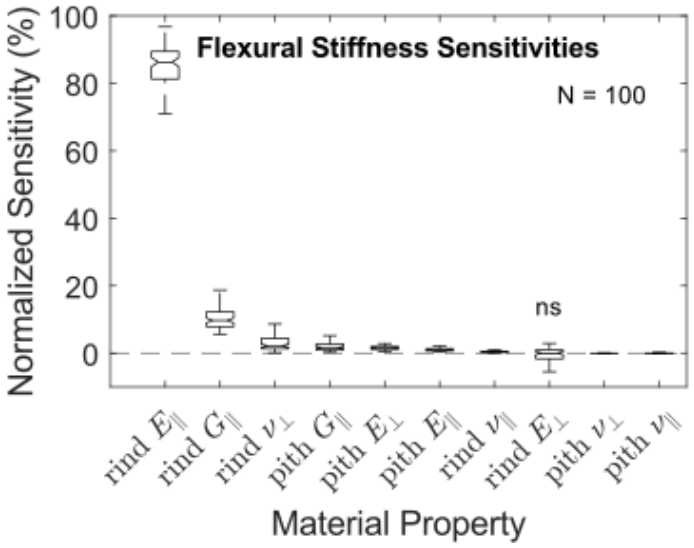

Figure 4.7: Flexural stiffness material property sensitivities (ranked).

Fig. 4.8 shows the ranked influence of material properties on failure strength. Failure strength was also most highly influenced by the elastic modulus of rind tissue parallel to the fibers (rind $E_{||}$). But unlike flexural stiffness, failure strength was more broadly influenced by other material properties, such as the elastic modulus of pith tissue transverse to the fibers (pith E) and the shear modulus of pith and rind tissue parallel to the fibers (rind and pith $G_{||}$). Distributions that were deemed statistically not significant (ns) from one sample t-testing ($p > 0.05$) are marked with an 'ns'.

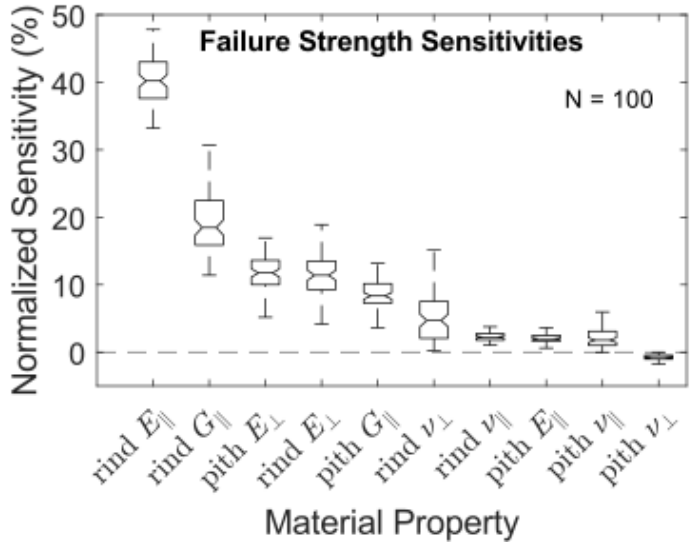

Figure 4.8: Failure strength material sensitivities (ranked).

4.3.2 Geometric Sensitivity Results

Fig. 4.9 shows the ranking of flexural stiffness, failure strength, and biomass sensitivities with respect to the first twenty principal components. Distributions that were deemed statistically not significant (ns) from one sample t-testing ($p > 0.05$) are marked with an 'ns'.

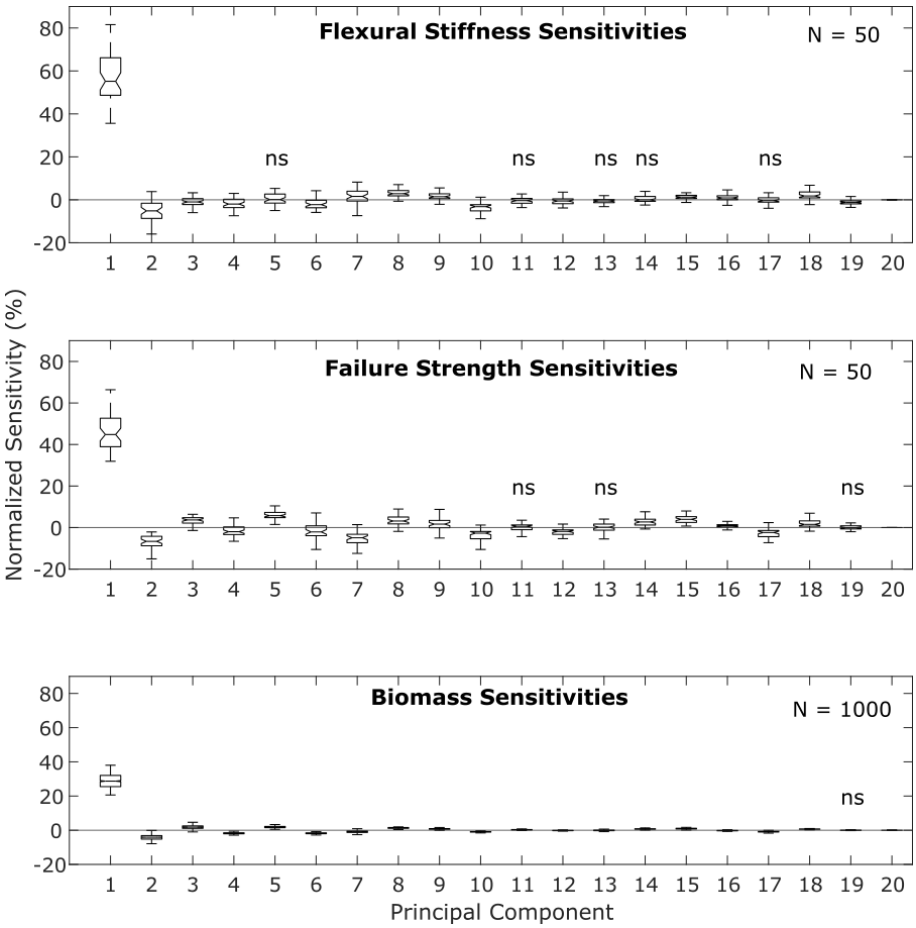

Figure 4.9: Calculated geometric sensitivities for flexural stiffness, failure strength and biomass with respect to the first twenty principal components. The number of samples for biomass sensitivities (1000) is different from the other sensitivities due to random sampling of pith and rind densities (see Section 4.2.5)

The first principal component had the highest influence on model flexural stiffness (median 55%), failure strength (median 45%), and biomass (median 27%). All other principal components had relatively low influence. For flexural stiffness sensitivities, all remaining principal components had median sensitivities below +/- 6%. For failure strength sensitivities, all other principal components had median sensitivities below +/- 7%. For mass sensitivities, all other principal components had median sensitivities below +/- 4%.

Uncertainty in the value of pith density and rind density were found to have little effect on the biomass sensitivities shown in Fig. 4.9. An uncertainty analysis revealed that for each principal component

sensitivity, the maximum error due to density uncertainty was less than +/- 0.5 percent normalized sensitivity. This was a small enough error that error bars were not included for biomass sensitivities in Fig. 4.9.

4.3.3 Relationships between Mass and Flexural Stiffness/Failure Strength Sensitivities

Fig. 4.10 shows a scatter-plot between biomass sensitivities and flexural stiffness sensitivities / failure strength sensitivities. Both plots show positive correlations between stiffness / strength and biomass. The cluster of data around the origin of these charts shows that all other principal component sensitivities (in various colors) had much weaker relationships with biomass sensitivities.

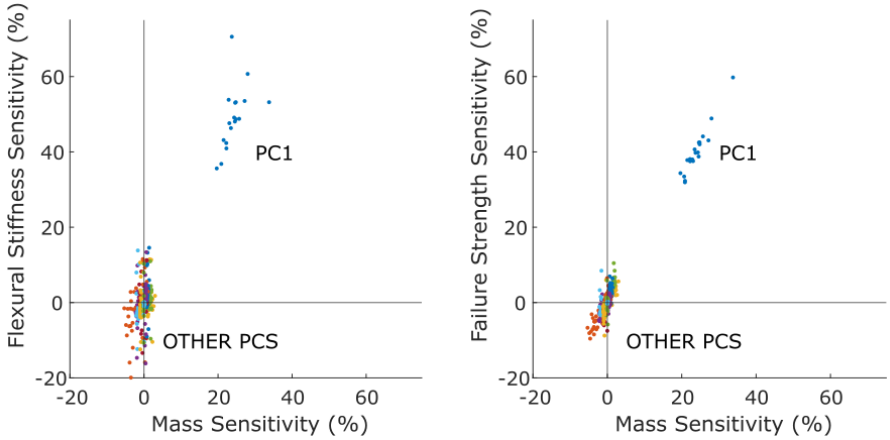

Figure 4.10: Scatter plots of mass sensitivities to flexural stiffness/failure strength sensitivities. The first principal component sensitivities are shown in blue, and all other principal component sensitivities are shown in various colors.

4.3.4 Statistical Analysis of Full and Reduced Parameterized Models

Fig. 4.11 shows the linear model equations and r^2 statistics comparing 'reduced' parameterized models and 'full' parameterized models. The sensitivity results from Section 4.3.2 indicated that only the first principal component is distinguishable from the other principal components for flexural stiffness, failure strength, and biomass calculations. As such, the 'reduced' parameterized model was formed with only the first principal component present. The results of this analysis indicated that 95% of flexural stiffness, 86% of failure strength, and 95% of biomass can be predicted in parameterized stalk models using only the first principal component. The scatter plots for these relationships are shown in Fig. 4.11.

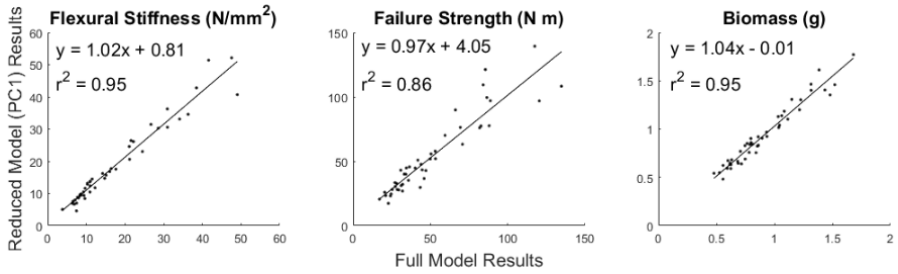

Figure 4.11: Full and reduced parameterized model comparison. The x-axis in each case is the quantity calculated by the 'full' parameterized model (with all principal components included) and the y-axis is the quantity calculated by the 'reduced' parameterized model (with only the first principal component).

4.3.5 Statistical Analysis of Principal Components and Maize Stalk Behavior

We now pivot from modeling results to statistical analysis of empirical data (as outlined in Section 4.2.8). Fig. 4.12 shows the relationships between actual maize stalk failure strength, the first principal component as it was extracted from the physical geometry of maize stalks, and section modulus of real maize stalk cross-sections. All relationships were fit with 3rd order polynomials. Both the first principal component and section modulus are very strong predictors of stalk strength ($r^2 = 0.8$). The relationship between the first principal component and section modulus was extremely strong ($r^2 = 0.96$). This indicates that the first principal component is essentially the same construct as the section modulus. All other principal components exhibited r^2 values of less than 0.01.

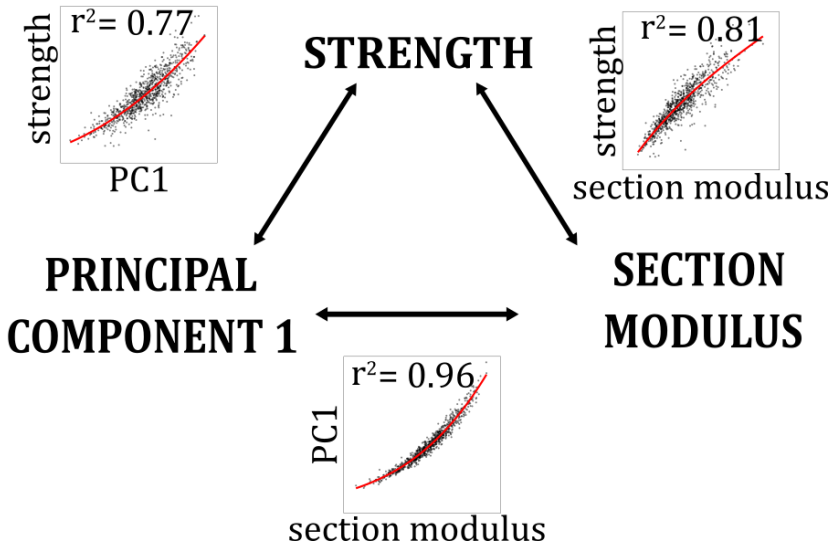

Figure 4.12: Comparisons between maize stalk failure strength, principal component 1, and section modulus. The fit lines shown are third order fits.

4.4 Discussion

4.4.1 Material Sensitivities

Material sensitivity analysis provided similar results to previous studies [10]. The most influential material property for both flexural stiffness and failure strength analyses was the longitudinal modulus of the rind tissue (rind $E_{||}$). Higher variation in material sensitivities was observed for failure strength, which is similar to the phenomenon observed in past studies [18]. This is likely the case because failure modeling is a complicated phenomenon dependent on more factors than static analysis [24].

[10] Stubbs *et al.*, "Maize stalk stiffness and strength are primarily determined by morphological factors," 2022.

[18] Ottesen *et al.*, "Development and stochastic validation of a parameterized model of maize stalk flexure and buckling," 2023.

[24] Hitchings *et al.*, *NAFEMS: An Introduction to Modeling Buckling and Collapse*, 2007.

4.4.2 Geometric Sensitivities

Geometric sensitivity analysis revealed that the first principal component had high sensitivity values for flexural stiffness, failure strength, and biomass. All other principal components had low sensitivity values. These results indicate that the majority of stalk behavior is influenced by only the first principal component.

The results shown in Fig. 4.10 further confirm this point. Looking at Fig. 4.10, it is obvious that the first principal component stands apart from all other principal components. The other principal components are barely distinguishable from each other, and are centered near (0,0).

The fact that there is only one influential factor that influences model behavior suggests that mass constrained optimization studies concerning 3D parameterized maize stalk models using principal components as factors may not be feasible. This is because constrained optimization usually requires multiple influential factors, whereas the 3D parameterized model only has one. We had hoped that this sensitivity analysis would suggest strategies for increasing stalk strength without increasing biomass. Unfortunately, these results suggest that there is little possibility of increasing stalk strength without increasing biomass. As shown in Fig. 4.10, when strength increases, it is virtually always accompanied by an increase in biomass.

Lastly, because the maximum error uncertainty in biomass sensitivities was less than +/- 0.5, we can conclude that uncertainty in pith and rind densities does not affect the results of this chapter. The estimated pith and rind densities had distributions with high variation and were only 'ballpark' estimates. Fortunately, the accuracy of density estimates did not significantly affect our biomass sensitivity calculations.

4.4.3 Reduced Models and Principal Components

Statistical analysis between 'reduced' parameterized models that only contained the first principal component and 'full' parameterized models that contained all principal components revealed that 85% of model failure strength can be predicted by only the first principal component. This indicates that the geometric behaviors quantified by the other principal components associated with stalk geometry have little impact on strength. The geometric behavior associated with the first principal component, however, is the primary determinant of stalk strength.

4.4.4 Section Modulus

Prior to this paper, the relationship between maize stalk strength and section modulus was based on purely observational "mechanics-based regression" [8]. This approach used insights from structural mechanics to inform the regression approach. The structural quantity of section modulus was found to be the strongest predictor of stalk strength. In a similar manner, flexural stiffness was also found to be a good predictor of stalk strength.

[8] Robertson *et al.*, "Maize Stalk Lodging: Morphological Determinants of Stalk Strength," 2017.

A single principal component was found to be closely related to flexural stiffness, stalk strength, and biomass. Principal component analysis is a purely statistical approach that identifies natural patterns in data sets without making any prior assumptions about the resulting patterns. Modification of the principal components through sensitivity analysis demonstrated that the first principal component had a strong influence on flexural stiffness, stalk strength, and biomass. In addition, the remaining principal components had very little influence on the stiffness, strength, and biomass. This finding was reinforced by creating reduced models that included the first principal component but omitted all other components. These reduced models produced results that were extremely close to the results of models that included all principal components Fig. 4.11.

As a purely statistical method, principal component analysis doesn't "know" anything about structural mechanics. Yet the first principal component was found to be extremely closely related to the section modulus ($r^2 = 0.96$). The analysis therefore provides independent support for the idea that section modulus is the primary predictor of stalk strength. In other words, a purely statistical approach (principal component analysis) and mechanics-based regression provided independent paths to the same conclusions.

4.4.5 Limitations

Several limitations affect the results of this chapter. For one, there are several side effects to quarter-symmetric models. Calculated buckling modes can no longer be antisymmetric [24], and therefore can no longer occur on the bottom part of a modeled stalk. Also, any calculated values such as flexural stiffness or failure moment are half the value of their full-model counterparts. These problems can be remedied by adjusting output values for quarter-symmetric models by a factor of two. Several limitations affect the results of this chapter. For one, there are several side effects to quarter-symmetric models. Calculated buckling modes can no longer be antisymmetric [24], and therefore can no longer occur on the bottom part of a modeled stalk. Also, any calculated values such as flexural stiffness or failure moment are half the value of their full-model counterparts. These problems can be remedied by adjusting output values for quarter-symmetric models by a factor of two.

[24] Hitchings *et al.*, *NAFEMS: An Introduction to Modeling Buckling and Collapse*, 2007.

[24] Hitchings *et al.*, *NAFEMS: An Introduction to Modeling Buckling and Collapse*, 2007.

The models were also based on fully matured, dried, healthy maize stalks. This means that the calculated sensitivities are only applicable

to stalks of a similar caliber. Because maize stalks have been known to behave differently when unhealthy, moist, or during different stages of development [16, 63], these sensitivities will likely be affected by any changes to stalk condition.

Sensitivities were also calculated within 25% of a standard deviation of either principal component coefficients or material properties. This means that these sensitivities are only accurate within this range. The models may behave differently outside of this range. In spite of this, we believe that keeping to within 25% of a standard deviation for the relevant quantities is important to preserve behaviors of maize stalks seen in nature, and that going outside of this bound may lead to inaccuracies.

[16] Sutherland *et al.*, "The Influence of Water Content on the Longitudinal Modulus of Elasticity of Maize Stalk Tissues," 2022.

[63] Xue *et al.*, "Physiological Influence of Stalk Rot on Maize Lodging after Physiological Maturity," 2021.

5 Summary and Conclusion

5.1 Summary of Results

The purpose of this study was to improve and better understand the factors that influence maize stalk failure. First, the process for creating and analyzing 3D parameterized finite-element models of maize stalks was automated. Second, the longitudinal shear modulus of maize stalk pith and rind tissues were measured to fill a gap in our current set of material constants used in FEA analysis. Third, a sensitivity analysis was performed to assess the influence of material and geometric factors on maize stalk flexural stiffness, failure strength, and biomass.

The creation and analysis of 3D parameterized models in FEA were automated using the python/Abaqus API, which allows for complete user control over boundary conditions, meshes, and geometries. The created automated package can now create a model in under one minute. This is a major improvement over the 20 minutes previously required when manually creating a model. Validation of the automated package showed high correlation between simulation results and results from physical testing, with an r^2 of 0.98 for flexural stiffness, and an r^2 of 0.73 for failure strength [18]. The automated modeling platform supports the automated creation of models that can be used for sensitivity analyses and optimization studies.

[18] Ottesen *et al.*, "Development and stochastic validation of a parameterized model of maize stalk flexure and buckling," 2023.

The transverse shear modulus of maize pith and rind tissue were measured for dry and fully mature maize stalks. The shear modulus of the rind tissue had a mean of 931 MPa and standard deviation of 334 MPa. The pith shear modulus had a mean of 27 MPa and standard deviation of 10 MPa. Rind measurements had similar values to bamboo and wood. These measurements are the first reported values in the literature. Their use in FEA models allows researchers to avoid the estimation process that was necessary before these measurements were taken.

The automated model generation package was used to perform a sensitivity analysis in order to assess the influence of material and geometric factors on model flexural stiffness, failure strength, and biomass. Sensitivity analysis consisted of making changes to statistical geometric patterns found in actual maize. These statistical geometric patterns were found using principal component analysis. Manipulating the principal component patterns increased the 'amount' of a particular pattern found in actual maize. Results indicated high failure strength sensitivity to the first principal component, with low sensitivity to all other principal

components. The first principal component is highly correlated with section modulus ($r^2 = 0.97$); this is independent validation that section modulus is the primary predictor of stalk strength, which is consistent with previous studies [8]. Results indicated that all failure strength sensitivities had positive correlations with biomass. Because there is only one influential predictor of stalk strength, and because all model parameter failure strength sensitivities are positively correlated with biomass sensitivities, it is unlikely that future optimization analyses using the principal component patterns in this study could result in stalks with higher failure strength without increasing biomass.

[8] Robertson *et al.*, "Maize Stalk Lodging: Morphological Determinants of Stalk Strength," 2017.

5.2 Contributions

The automated system described in Chapter 2 supported a study focused on validating the parameterized maize stalk model. The validation study was published in the journal *Plant Methods* and I was a co-author on that paper [18]. The automated system also contributed to the material and geometric sensitivity analysis in Chapter 4.

The measurement of longitudinal shear modulus of pith and rind tissue in Chapter 3 resulted in a paper that has been accepted for publication in the journal *Plant Methods* [25], These results were subsequently used in the models described in Chapter 4.

The sensitivity analysis in Chapter 4 has been submitted to the journal *in Silico Plants*. These results will also inform future studies concerning the effect of geometric parameters on stalk response.

[18] Ottesen *et al.*, "Development and stochastic validation of a parameterized model of maize stalk flexure and buckling," 2023.

[25] Carter *et al.*, "Measurement of Maize Stalk Shear Moduli," 2023.

5.3 Future Work

Several future studies would be beneficial to complement the work done in this thesis. Firstly, now that a solid relationship has been established between principal components and model response, optimization studies could be performed to improve model failure strength by manipulating the principal components rather than individual model parameters. Based on the results of the sensitivity analysis, it seems unlikely that model failure strength can be increased significantly without increasing biomass. This is because the sensitivity analysis revealed only positive correlations between failure strength and biomass. However, an optimization study that does not constrain biomass could quantify the degree of biomass increase; it may be that the tradeoff between increasing stalk biomass and increasing stalk strength is small enough to warrant attention in selective breeding.

Second, if stalk strength cannot be feasibly increased with additional biomass, future studies will need to focus on increasing stalk strength in other ways. While this thesis sought to preserve variation patterns found in nature (through principal component analysis), it may be the case that breaking these patterns may allow for increases in failure strength without significantly increasing biomass. The downside to this approach

is that it may indicate an optimal solution that is difficult or impossible to achieve through natural breeding.

In addition to optimization studies, further work could focus on some factors that are currently ignored in our models. For example, our models only model a small portion of maize stalks (about 50 millimeters above and below a single node) instead of the entire stalk. In addition, our models do not include the leaf sheath, which has been found to be influential in stalk failure [64]. Lastly, our models do not include the relationship between stalks and the soil. The addition of each of these factors would lead to a more comprehensive model. Fortunately, the current model provides a flexible platform upon which these additional capabilities could be built. Thus it is hoped that this model will both be used in future studies in its current form and expanded upon to increase its capabilities.

[64] Ogilvie *et al.*, "Effects of the Leaf Sheath on Stalk Strength in Maize," 2024.

5.4 Conclusions

The results of this thesis are 1) an automated modeling package that allows models of any desired shape and material properties to be created approximately 100 times faster than previously possible; 2) distributions of longitudinal shear modulus of pith and rind tissue, found to be 13 MPa to 55 MPa for pith tissue and 355 MPa to 1630 MPa for rind tissue; and 3) evidence that the strength and flexibility of maize stalks are governed by a single mode of geometric variation, which is positively correlated with biomass and closely related to section modulus. These findings significantly contribute to the field of engineering in agronomy, and help researchers better understand the factors that contribute to maize stalk lodging.

References

[1] USDA, "Grain: World Markets and Trade," 2024. cited on p. 1

[2] USDA, "Feed Grains Sector at a Glance," 2023. cited on p. 1

[3] Energy, U. D. of, "Ethanol Fuel Basics," 2024. cited on p. 1

[4] Duvick, D. N., "The Contribution of Breeding to Yield Advances in maize," *Advances in Agronomy*, vol. 86, 2005, pp. 83–145. cited on p. 1

[5] Thompson, J. L. and Tyner, W. E., "Corn stover for bioenergy production: Cost estimates and farmer supply response," *Biomass and Bioenergy*, vol. 62, 2014, pp. 166–173. cited on p. 1

[6] Robertson, D., Smith, S., Gardunia, B., and Cook, D. D., "An Improved Method for Accurate Phenotyping of Corn Stalk Strength," *Crop Science*, 2014. cited on p. 1

[7] Von Forell, G., Robertson, D., Lee, S., and Cook, D., "Preventing lodging in bioenergy crops: A biomechanical analysis of maize stalks suggests a new approach," *Journal of Experimental Botany*, vol. 66, no. 14, 2015, pp. 4367–4371. cited on pp. 1–3, 34

[8] Robertson, D., Julias, M., and Cook, D. D., "Maize Stalk Lodging: Morphological Determinants of Stalk Strength," *Crop Science*, 2017. cited on pp. 1, 34, 46, 52, 55

[9] Ottesen, M., Larson, R., Stubbs, C., and Cook, D., "A parameterised model of maize stem cross sectional morphology," English, *Biosystems Engineering*, vol. 218, 2022, pp. 110–123. cited on pp. 2–4, 7, 14, 21–23, 38, 40

[10] Stubbs, C., Larson, R., and Cook, D., "Maize stalk stiffness and strength are primarily determined by morphological factors," 2022. cited on pp. 2, 3, 10, 14, 22, 32, 34, 38, 40, 41, 51

[11] Ottesen, M., Carter, J., Hall, R., Liu, N.-W., and Cook, D., "Development and Stochastic Validation of a Parameterized Model of Maize Stalk Flexure and Buckling," *In Silico Plants*, 2023. cited on pp. 2, 7

[12] Hashmi, S., Van Tyne, C. J., Batalha, G. F., and Yilbas, B., *Comprehensive Materials Processing*. 2014. cited on p. 2

[13] Al-Zube, L., Wenhuan, S., Robertson, D., and Cook, D., "The elastic modulus for maize stems," *Plant Methods*, 2018. cited on pp. 2, 4, 10, 11, 14, 21, 22, 33, 41, 44, 46

[14] Zhang, L., Yang, Z., Zhang, Q., and Guo, H., "Tensile Properties of Maize Stalk Rind," 2016. cited on pp. 2, 21, 22, 33

[15] Zhang, L., Yang, Z., Zhang, Q., Zhu, X., and Hu, H., "Mechanical Behavior of Corn Stalk Pith: An Experimental and Modeling Study," 2017. cited on pp. 2, 21, 22

[16] Sutherland, B., Steele, K., and Cook, D., "The Influence of Water Content on the Longitudinal Modulus of Elasticity of Maize Stalk Tissues," 2022. cited on pp. 2, 10, 21–23, 32, 33, 41, 53

[17] Robertson, D., Lee, S. Y., Julias, M., and Cook, D. D., "Maize Stalk Lodging: Flexural Stiffness Predicts Strength," *Crop Science*, 2016. cited on pp. 2, 12, 14, 40

[18] Ottesen, M., Carter, J., Hall, R., Liu, N.-W., and Cook, D. D., "Development and stochastic validation of a parameterized model of maize stalk flexure and buckling," *In silico Plants*, vol. 5, no. 2, 2023. cited on pp. 4, 5, 10, 11, 13, 14, 18, 23, 34, 36, 38, 41, 42, 51, 54, 55

[19] Al-Zube, L., Robertson, D., Edwards, J., Sun, W., and Cook, D., "Measuring the compressive modulus of elasticity of pith-filled plant stems," *Plant Methods*, 2017. cited on pp. 4, 10, 11, 14, 21, 22, 44

[20] Blokdyk, G., *Procedural Programming A Complete Guide*. 2020. cited on p. 8

[21] Green, D., Winandy, J., and Kretschmann, D., *Wood Handbook: Wood as an engineering material*. 1999. cited on pp. 10, 23, 31–33, 41

[22] Benzley, S. E., Perry, E., Merkley, K., Clark, B., and Sjaardama, G., "A Comparison of All Hexagonal and All Tetrahedral Finite Element Meshes for Elastic and Elasto-plastic Analysis," *4th international meshing roundtable*, 1995. cited on p. 13

[23] Hughes, T. J. R., *The Finite Element Method*. 1987. cited on p. 17

[24] Hitchings, D. and Falzon, B., *NAFEMS: An Introduction to Modeling Buckling and Collapse*. 2007. cited on pp. 51, 52

[25] Carter, J., Hoffman, J., Fjeldsted, B., Ogilvie, G., and Cook, D. D., "Measurement of Maize Stalk Shear Moduli," *Plant Methods*, 2023. cited on pp. 10, 21, 41, 55

[26] Boresi, A. and Schmidt, R., *Advanced Mechanics of Materials*, 6th ed. 2002. cited on pp. 21, 24

[27] Stubbs, C., Sun, W., and Cook, D., "Measuring the transverse Young's modulus of maize rind and pith tissues," *Journal of Biomechanics*, vol. 84, 2019, pp. 113–120. cited on p. 22

[28] Robertson, D., Smith, S., and Cook, D. D., "On Measuring the Bending Strength Of Septate Grass Stems," *American Journal of Botany*, 2015. cited on pp. 22–24

[29] Stubbs, C., Larson, R., and Cook, D. D., "Mapping spatially distributed material properties in finite element models of plant tissue using computed tomography," *Biosystems Engineering*, 2020. cited on pp. 22, 23

[30] , *ASTM E143-20: Standard Test Method for Shear Modulus at Room Temperature*. cited on p. 23

[31] Revelo, D. C., Papadopoulos, C., Costa, F. A., Harries, K. A., and Saffar, A., "Development of a Method to Test Bamboo Culms in Direct Torsion," 2022. cited on p. 23

[32] Askarinejad, S., Kotowski, P., and Rahbar, N., "Effects of humidity on shear behavior of bamboo," 2015. cited on p. 23

[33] Moran, R., Ghavami, K., and García, J., "A new method to measure the axial and shear moduli of bamboo," 2017. cited on pp. 23, 31, 32

[34] Brabec, M., Lagana, R., Milch, J., Tippner, J., and Sebera, V., "Utilization of digital image correlation in determining of both longitudinal shear moduli of wood at single torsion test," *Wood Science and Technology*, vol. 51, 2016, pp. 29–45. cited on p. 23

[35] Budynas, R. and Sadegh, A., *Roark's Formulas for Stress and Strain*, English, 9th ed. McGraw Hill, 2020. cited on pp. 24, 28

[36] Popov, E. P., Nagarajan, S., and Lu, Z. A., *Mechanics of Materials*, 2nd ed. 2015. cited on p. 24

[37] Nelson, N., Stubbs, C., Larson, R., and Cook, D. D., "Measurement accuracy and uncertainty in plant biomechanics." *Journal of Experimental Botany*, 2019. cited on p. 28

[38] Coleman, H. and Steele, G., *Experimentation, Validation, and Uncertainty Analysis for Engineers*. 2009. cited on p. 29

[39] Zabler, S., Paris, O., Burgert, I., and Fratzl, P., "Moisture changes in the plant cell wall force cellulose crystallites to deform," *Journal of Structural Biology*, vol. 171, 2010, pp. 133–141. cited on p. 33

[40] Rowell, R. and Skaar, C., *The Chemistry of Solid Wood; Advances in Chemistry*. 1984. cited on p. 33

[41] Oduntan, Y., Kunduru, B., Tabaracci, K., Mengistie, E., McDonald, A. G., Sekhon, R. S., and Robertson, D., "The effect of structural bending properties versus material bending properties on maize stalk lodging." *European Journal of Agronomy*, vol. 159, 2024. cited on p. 33

[42] Martin-Nelson, N., Sutherland, B., Yancey, M., Liao, C. S., Stubbs, C., and Cook, D. D., "Axial variation in flexural stiffness of plant stem segments: Measurement methods and the influence of measurement uncertainty," *Plant Methods*, vol. 17, 2021. cited on p. 33

[43] Hale, J., Webb, S., Stubbs, C., and Cook, D. D., "Assessing axial and temporal effects of the leaf sheath on the flexural stiffness of large-grain stems." *Crop Science*, vol. 63, no. 2, 2023, pp. 822–832. cited on p. 33

[44] Saltelli, A., Chan, K., and Scott, E. M., *Sensitivity Analysis*, 1st ed. Wiley, 2009. cited on p. 34

[45] Hamby, D. M., "A Comparison Of Sensitivity Analysis Techniques," *Health Physics*, 1995. cited on p. 34

[46] Richter, G. M., Acutis, M., Trevisiol, P., Latiri, K., and Confalonieri, R., "Sensitivity analysis for a complex crop model applied to Durum wheat in the Mediterranean," *European Journal of Agronomy*, vol. 32, no. 2, 2010. cited on p. 34

[47] Gao, Y., Song, C., Rao, X., and Ying, Y., "Image processing-aided FEA for monitoring dynamic response of potato tubers to impact loading," *Computers and Electronics in Agriculture*, vol. 151, 2018, pp. 21–30. cited on p. 34

[48] Confalonieri, R., Bellocchi, G., Bregaglio, S., Donatelli, M., and Acutis, M., "Comparison of sensitivity analysis techniques: A case study with the rice model WARM," *Ecological Modelling*, vol. 221, 2010, pp. 1897–1906. cited on p. 34

[49] Robertson, D., Julias, M., Gardunia, B., Barten, T., and Cook, D. D., "Corn Stalk Lodging: A Forensic Engineering Approach Provides Insights into Failure Patterns and Mechanisms," *Crop Science*, 2015. cited on p. 35

[50] Groen, E. A. and Heijungs, R., "Ignoring correlation in uncertainty and sensitivity analysis in life cycle assessment: What is the risk?" *Environmental Impact Assessment Review*, vol. 62, 2017, pp. 98–109. cited on p. 37

[51] Jackson, E. J., *A User's Guide to Principal Components*. 1991. cited on p. 37

[52] Schwarz, C., Ackert, P., and Mauermann, R., "Principal component analysis and singular value decomposition used for a numerical sensitivity analysis of a complex drawn part," *The International Journal of Advanced Manufacturing Technology*, vol. 94, 2018, pp. 2255–2265. cited on p. 38

[53] Xiao, M., Lu, D., Breitkopf, P., Raghavan, B., Dutta, S., and Zhang, W., "On-the-fly model reduction for large-scale structural topology optimization using principal components analysis," *Structural and Multidisciplinary Optimization*, vol. 62, 2020. cited on p. 38

[54] Ramsey, F. and Schafer, D., *The Statistical Sleuth: A Course in Methods of Data Analysis*, 3rd ed. 2013. cited on p. 38

[55] Milton, G. W., *The Theory of Composites*. 2002. cited on p. 40

[56] Touzani, R., *Finite Elements and Symmetry*. 2020. cited on p. 40

[57] Kumar, A. T. M. and Reddy, S., "Bending and Cutting Characteristics of Maize Stalk Residue," *Research Journal of Agricultural Sciences*, 2015. cited on p. 42

[58] Falzon, B. and Aliabadi, M. H., *Buckling and Postbuckling Structures*. 2008. cited on p. 42

[59] Saranpaa, P., *Wood Quality and its Biological Basis*. 2009. cited on p. 42

[60] Huang, P., Chang, W.-S., Ansell, M. P., Chew, Y. M. J., and Shea, A., "Density distribution profile for internodes and nodes of Phyllostachys edulis (Moso bamboo) by computer tomography scanning," *Construction and Building Materials*, vol. 93, 2015, pp. 197–204. cited on p. 42

[61] Särndal, C.-E. and Wretman, J., *Model Assisted Survey Sampling*. 2003. cited on p. 44

[62] Navidi, W., *Statistics for Engineers and Scientists*, 5th ed. 2020. cited on p. 46

[63] Xue, J., Gao, S., Hou, L., Li, L., Ming, B., Xie, R., Wang, K., Hou, P., and Li, S., "Physiological Influence of Stalk Rot on Maize Lodging after Physiological Maturity," *Agronomy*, vol. 11, 2021. cited on p. 53

[64] Ogilvie, G., Cook, D. D., Hall, R., Shamo, C., Hall, J., Smith, K., and Noh, C., "Effects of the Leaf Sheath on Stalk Strength in Maize," 2024. cited on p. 56